For submission to American Mineralogist (Revision 1):

Word Count: 9966

Microstructural changes and Pb mobility during the zircon to reidite transformation: implications for planetary impact chronology

Ian Szumila[1], Dustin Trail[1], Timmons Erickson[2],

Justin I. Simon[3], Matthew M. Wielicki[4], Tom Lapen[5],

Miki Nakajima[1], Marc Fries[3], Elizabeth A. Bell[6]

[1]Univesity of Rochester (iszumila@ur.rochester.edu), Earth and Environmental Science, Rochester, NY, [2]Jacobs - JETS, NASA Johnson Space Center, Houston, TX, 77058, USA, [3]Astromaterials Research and Exploration Science, NASA Johnson Space Center, Houston, TX 77058, USA, [4]University of Alabama, Department of Geological Sciences, Tuscaloosa, AL, 35487, USA, [5]University of Houston, Department of Earth and Atmospheric Sciences, Houston, TX 77004, USA, [6]University of California Los Angeles, Department of Earth, Planetary and Space Sciences, Los Angeles, CA 90095, USA

DOI: https://doi.org/10.2138/am-2022-8604. http://www.minsocam.org/

Abstract

Impact events modify and leave behind a complex history of rock metamorphism on terrestrial planets. Evidence for an impact event may be recorded in physical changes to minerals, such as mineral deformation and formation of high-P/T polymorphs, but also in the form of chemical fingerprints, such as enhanced elemental diffusion and isotopic mixing. Here we explore laboratory shock-induced physical and chemical changes to zircon and feldspar, the former of which is of interest because its trace elements abundances and isotope ratios are used extensively in geochemistry and geochronology. To this end, a granular mixture of Bishop Tuff sanidine and Kuehl Lake zircon, both with well-characterized Pb isotope compositions, was prepared and then shocked via a flat plate accelerator. The peak pressure of the experiment, as calculated by the impedance matching method, would be ~24 GPa although a broader range of *P-T* conditions is anticipated due to starting sample porosity. Unshocked and shocked materials were characterized via Scanning Electron Microscopy (SEM), Electron Backscatter Diffraction (EBSD), and Raman spectroscopy. These methods show that the starting zircon material had abundant metamict regions, and the conversion of the feldspar to glass in the post-shock material. Analyses of the shocked product also yielded multiple occurrences of the high pressure $ZrSiO_4$ polymorph reidite, with some domains up to 300 μm across. The possibility of U-Pb system disturbance was evaluated via Laser Ablation-Inductively Coupled Plasma-Mass Spectrometry (LA-ICP-MS) and Secondary Ion Mass Spectrometry (SIMS). The isotopic data reveal that disturbance of the U-Pb geochronometer in the reidite was minimal (<2% for the main U-Pb geochronometers). To better constrain the *P-T* conditions during the shock experiment, we complement impedance matching pressure calculations with iSALE2D impact simulations. The simulated results yield a range of *P-T* conditions experienced during the experiment and show that much of the sample may have reached >30 GPa, which is consistent with formation of reidite. In the recovered shocked material, we identified lamellae of reidite, some of which interlock with zircon lamellae. Reidite {112} twins were identified, which we interpret to have formed to reduce stress between the crystal structure of the host zircon and reidite. These two findings support the interpretation that shear transformation enabled the transition of zircon to reidite. The size and presence of reidite found here indicate that this phase is probably common in impact-shocked crustal rocks that experienced ~25 to ~35 GPa, especially when the target material has porosity. Additionally, shock loading of the zircon and transformation to reidite at these pressures in porous materials is unlikely to significantly disturb the U-Pb system in zircon and that the reidite inherits the primary U and Pb elemental and isotopic ratios from the zircon.

Keywords: impact, flat-plate shock experiments, zircon, reidite, sanidine, U-Pb dating

Introduction

Impact craters are common features of terrestrial planets and moons and are even more common than just observation indicates. Craters may be overprinted by later impacts or destroyed by geodynamic/hydrologic activity on bodies like Earth. Thus, in addition to searching for geomorphic evidence of past impact craters, these challenges have led researchers to explore in detail the chemical and mineralogical record of material affected by impact processing. To confirm an impact crater origin, detection of shock metamorphosed material at the impact site or in related ejecta, or the detection of meteoritic material is usually required (French and Koeberl, 2010). Minerals from impacted terrains may show chemical or structural changes due to shock, where information preserved in these features can be used to study the details of the hypervelocity event. The microstructures detected in shocked zircon at the Vredefort Dome, for example, help to understand the shock loading experienced during this impact (e.g. Moser et al., 2011; Erickson et al., 2013). Preserved mineralogic characteristics include shock metamorphism-induced structural changes, such as transition of zircon to the high-pressure polymorph reidite (Glass and Liu, 2001), or chemical changes such as increased element mobility (e.g. Reddy et al., 2016) that could disturb a sample's U-Pb isotope system.

Reidite, a high-pressure polymorph of zircon, is ~10% denser than zircon (Kusaba et al., 1986) with a scheelite-type structure (Liu, 1979) and has been identified at terrestrial impact structures and ejecta deposits. For example, it was identified in an Eocene impact ejecta layer considered likely to have been sourced from the Chesapeake Bay impact structure (Glass and Liu 2001; Glass et al., 2002; Wittmann et al., 2006) A $ZrSiO_4$ grain found in the ejecta was about 90% reidite and 10% relict zircon (Cavosie et al., 2021). Reidite has also been identified at the Ries impact structure (Gucsik et al., 2004a; Erickson et al., 2017), the Xiuyan impact structure (Chen et al., 2013), the Rock Elm impact structure (Cavosie et al., 2015), the Woodleigh impact structure (Cox et al., 2018), and within the Stac Fada Member, helping to confirm an impact origin for the deposit (Reddy et al., 2015). The phase has even been discovered in a lunar meteorite (Xing et al., 2020). Reidite has been produced in the laboratory via both static loading (Reid and Ringwood, 1969) and shock loading experiments (Kusaba et al., 1986, Leroux et al., 1999) but at different pressures for each kind of experiment. The exact mineral transformation mechanism relevant for zircon and reidite is further explored in the discussion. The first hydrostatic experiments determined that zircon is fully converted to a scheelite-type phase (i.e. reidite) around 900 °C (1173 K) and 12 GPa (Reid and Ringwood 1969). Experiments done with a diamond anvil cell (DAC) apparatus produced reidite at 19.7 GPa (Westenren et al., 2004) or ~23 GPa (Knittle and Williams, 1993), whereas thermodynamic calculations predict the transition lies between ~8 and 12 GPa (Akaogi et al., 2018). Ono et al. (2004) produced reidite at 8.7 ± 1 GPa and 927 °C (1200 K) using a multi-anvil press. However, shock-loading experiments have not produced reidite below ~30 GPa (Kusaba et al., 1985). Leroux et al. (1999) studied zircon experimentally shocked to peak pressures of 20, 40 and 60 GPa. Their 20 GPa experiment showed only deformation effects, their 40 GPa experiment showed partial conversion to reidite, and at 60 GPa full conversion to reidite was detected. They also identify twins with (112) habit plane for the reidite material in their 40 and 60 GPa experiments. Reversion of reidite to zircon at 1 atm was shown to occur after samples reached 1200 °C (1473 K) with a heating rate of 40 °C/min (Kusaba et al., 1985).

Physical changes of shocked zircon (e.g., phase transitions and twinning) can be accompanied by chemical disturbances. Uranium or Pb mobility due to impact processes (whatever the physical mechanism) could alter the apparent U-Pb crystallization age of a mineral. Some zircons taken from the Vredefort dome, for example, appear to have lost Pb and these grains have possibly experienced shock-related age resetting (Wielicki and Harrison, 2015; Moser et al., 2011; Cavosie et al., 2016). Vredefort material containing zircon from around 25 km from the center of the dome was not reset in age, whereas zircon from within 15 km dome center did have its age disrupted, with some of this driven by Pb diffusion along impact generated defects (Moser et al., 2011). The extent of Pb loss experienced in Vredefort zircons is related to their shock morphology (Moser, 1997; Moser et al. 2011). Likewise, zircons derived from ejecta related to the Chicxulub impact event have shock features and isotopic resetting (Krogh et al., 1993) and plot on a mixing line between the time of the impact and the age of the basement rocks (Krogh et al., 1993). Krogh et al. (1993) also found that the degree of isotopic resetting in the zircons was related to their shock morphology, with the more shocked material plotting closer to the time of the impact event. More recently the U-Pb systematics of shocked zircons in Chicxulub's peak ring have been characterized by Rasmussen et al. (2019). While the zircons preserved U-Pb ages from Paleozoic all the way to the time of the impact, highly metamict regions in their fractured zircons preserved an age identical, within uncertainty, to the time of the Chicxulub impact itself. For Chicxulub zircons, the effective shock pressure experienced by zircons has been correlated to the density of their mineral hosts. Mineral hosts with densities with <3 g/cm^3 such as quartz or feldspar could amplify the shock pressure of 17.5 GPa experienced by a zircon to ~24 GPa (Wittmann et al., 2021).

Knowledge of the characteristics of impact shocked material will enable a better understanding of impact ages, and the changing impact flux through the evolution of the Solar System (e.g. Moser et al., 2019). This is particularly significant for extraterrestrial materials of which there are limited samples, and which often lack petrologic context. For example, partial Pb loss and variability, possibly induced by impacts, may contribute to the age spectrum of lunar zircons (Crow et al., 2017; Thiessen et al., 2018). Some lunar zircons, due to impact-related deformation, may have experienced Pb-loss or resetting of the U-Pb system associated with an impact-related thermal pulse (Pidgeon et al., 2007; Nemchin et al., 2009; Bellucci et al., 2016). The range in U-Pb ages for lunar zircons has been used to infer an impact event at ~4.2 Ga

(Zhang et al., 2012; Thiessen et al., 2018) and clustering of the lunar zircon $^{207}Pb/^{206}Pb$ ages at other specific dates before 4.0 Ga has suggested the possibility of other large impacts at various points in the evolution of the Moon (Hopkins and Mojzsis, 2015; Crow et al., 2017; Trail et al., 2020). Therefore, to extract accurate information out of U-Pb ages from ancient extraterrestrial zircons, a robust understanding of how shock affects Pb isotope mobility in zircon is fundamental. Here, we report the results of a mixture of sanidine and zircon —each with distinct Pb isotopic compositions— experimentally shocked via flat-plate accelerator. We identify the high-pressure polymorph of zircon, reidite in our post-shock material and analyze it from chemical and structural perspectives. For U-Pb geochronometers in reidite, we find larger variations in the measurements but limited difference when compared to the unshocked intact zircon. The average SIMS measurements of the U-Pb and Pb-Pb are consistently lower than for the zircon but never by more than 2% from that of the U-Pb systematics of the host zircon. Statistical tests indicate there is no evidence that the ages and U-Pb and Pb-Pb ratios are drawn from different distributions. Additionally, no contribution of Pb from the feldspar to the reidite grain is found.

Materials and methods

Starting materials

A syenitic rock was sourced from near Kuehl Lake (KL), Ontario, Canada with large zircons up to ~1 cm measured along the c-axis. One of these zircon grains was extracted for use in the shock experiment. The KL region is the source of the well-known 91500 zircon standard that been extensively characterized for trace element contents and isotope ratios (Wiedenbeck et al., 1995). We refer to the zircon material used in this experiment as KL zircon, denoting its provenance. We also obtained LV51 sanidine ($KAlSi_3O_8$) from the Bishop Tuff (BT) to be shocked along with the zircon material. This material has been well characterized with Pb isotopic analyses yielding a mean $^{207}Pb/^{206}Pb$ of $0.81813 \pm 1.2 \times 10^{-5}$ (the LV51 material used here is from the same hand sample as Simon et al., 2007). The Bishop Tuff is ca. 767 ka as obtained by zircon U-Pb geochronology and consistent with Ar-Ar dates from sanidine (Mark et al., 2017, Crowley et al., 2007). Both materials were individually crushed in a mortar and pestle and sieved to grain sizes between 125 to 250 μm using a mesh net sieve. The experiment used a mixture of 97 wt% sanidine, and 3 wt% zircon or approximately 0.155 g sanidine, and 0.005 g zircon.

Flat-plate impact experiment and *P-T* modeling

The mixed material was shocked at NASA Johnson Space Center (JSC) using the flat plate accelerator in the Experimental Impact Laboratory. A stainless-steel target assembly was produced with a sample well with a 1 cm diameter and 0.7 mm depth. The densities and amount of zircon and sanidine materials used and the volume of the sample well imply the pre-impact experiment porosity was ~70%, similar to estimates for the upper layer of lunar regolith (~83%; Hapke and Sato, 2016). The flyer plate was ~20 mm in diameter, ~2 mm thick and made of stainless steel. The blast chamber holding the sample target of the flat plate accelerator was evacuated to 143 mTorr. The target pressure for the shock-loading experiment was 25 GPa. Based on the final measured velocity of the flyer plate (1.132 km/s) and impedance matching calculations (Gibbons and Ahrens, 1971; Gibbons, 1974), the peak sample pressure would have been ~23.5 GPa, if the sample did not have high porosity. Post-experiment grain fragments were mounted in epoxy, which was polished with sandpaper, 1 μm alumina, and finished with a 50 nm colloidal silica dispersion.

The peak pressure experienced during a flat-plate accelerator experiment can be calculated using the impedance matching method if the Hugoniot of the flyer plate is known (Gibbons, 1974) but there are two limitations. First, it does not account for the target material being porous. Second, it does not provide information on the temperatures the sample experienced. Porous (granular) samples shocked via flat-plate accelerator typically see shock related deformation features and melting at lower pressures (as calculated by the impedance matching method) than fully crystalline materials. This was characterized by a campaign that shocked both crystalline lunar basalt discs (Schaal and Hörz, 1977) and granular lunar basalt sieved to different grain sizes (Schaal et al., 1979). Therefore, we also modeled the experiment computationally using iSALE2D to elucidate the *P-T* conditions that the sample experienced. The iSALE2D software package (Wünnemann et al., 2006) based on the SALE hydrocode (Amsden et al., 1980) was used to simulate the conditions of the impact shock flat-plate accelerator experiment. Measuring P-T conditions in the simulation was done by using tracer particles which can record *P-T* and other variables for each timestep with one timestep being equal to 0.1 μs in this simulation. Additional information on the methods and parameters used to generate the simulation are available in the supplemental online material (SOM). We compare computational *P-T* results from the simulation with our post-shock experiment mineralogy. Some amplification of the effective shock pressure experienced by the zircon is expected since the zircon material is being hosted in a lower-density feldspar (Wittmann et al., 2021).

This is the peer-reviewed, final accepted version for American Mineralogist, published by the Mineralogical Society of America.
The published version is subject to change. Cite as Authors (Year) Title. American Mineralogist, in press.
DOI: https://doi.org/10.2138/am-2022-8604. http://www.minsocam.org/

Analytical strategy

Pre- and post-shock material was analyzed via SEM, EBSD, Transmission EBSD, Raman spectroscopy, LA-ICP-MS, and SIMS. These techniques were used to characterize crystallinity and structure and to investigate the material for chemical (e.g. Pb isotopic) changes between the unshocked and post-shock material. Details on the methods and parameters for each type of analyses conducted can be found in the SOM. For averaged datasets, errors are reported as 2 times the propagated standard error (s.e.) of the average. If only one datapoint was analyzed for a particular dataset, then as 2 times the s.e. of that individual distribution. Uranium-Pb concordia diagrams were generated with the Isoplot® software package (Ludwig, 2003).

Results

SEM observations

Backscattered electron (BSE) images of the shocked product show evidence for melting of the feldspar, and fusion with zircon to a more cohesive material (**Figure 1**) than the granular pre-shock material. To make referencing our experimental products easier, we refer to the $ZrSiO_4$ pictured at the large upper right backscatter bright region in **Figure 1a** as grain A, the lower left backscatter bright region in **Figure 1b** as grain B, and the grain pictured in **Figure 1c** as grain C. Inspection of these SEM images shows other modifications from the experiment that occurred; fused zircon-sanidine regions of the sample, for instance, contain a darker region (seen in **Figure 1a**) that appears to be enriched in Si. Other SEM images including unshocked sanidine and unshocked zircon can be found in the SOM. Certain BSE bright points can be seen in the shocked zircon product (see **Figure 1b**). These were identified as U-Th oxides and can be found in unshocked starting materials as well, so they represent a phase that survived the shock experiment. A close-up of this U-Th material located on shocked $ZrSiO_4$ identified as grain B is presented in the SOM with an energy dispersive X-ray spectroscopy (EDS) chemical analysis.

Raman spectroscopy

Raman spectroscopy enables phase identification and broad characterization of damage to crystal structures. The Raman analysis on unshocked sanidine spectrum shows Raman bands at 480 cm^{-1} or 515 cm^{-1} (**Figure 2a** bottom spectrum). Feldspars can be distinguished by a strong band from 500 to 515 cm^{-1} with the position varying systematically depending on feldspar composition (Mernagh, 1991). A 514 cm^{-1} position is a good indication of sanidine. Post-impact “sanidine” shows a smooth spectrum indicating that the crystal structure was amorphized into diapletic glass (Ostertag, 1983; **Figure 2a** top spectrum). Since this material is derived from the LV51 sanidine but the Raman analyses indicates that post-experiment it does not possess a sanidine crystal structure, it is hereafter referred as shocked $KAlSi_3O_8$. In **Figure 2b** the bottom spectrum (black line) from the pre-shock intact zircon shows prominent zircon bands. Major bands at 439 cm^{-1}, 974 cm^{-1}, 1008 cm^{-1}, which are related to the stretching and vibrational modes of SiO_4 in zircon, are present (Gucsik et al., 2004b) Additionally there are bands for this spectrum near 356 cm^{-1}, 225 cm^{-1}, and 202 cm^{-1} which are related to lattice modes of zircon (Gucsik, 2007). The top spectrum in **Figure 2b (**green line) was collected from grain A. This material shows bands that distinguish it as reidite. The bands at 298 cm^{-1}, 327 cm^{-1}, 407 cm^{-1} are consistent with lattice vibrational modes of $ZrSiO_4$ but with a scheelite-type structure.

Additionally, an identifiable band near 847 cm^{-1} is related to a strain mode of reidite (Gucsik, 2007).

A Raman spectral map (**Figure 3**) of a sectioned half of the unshocked starting zircon grain suggests portions of this grain are metamict. This is probably due to radiation damage accumulated from high U-Th oxide material. Distinct regions on the unshocked zircon can be identified: intact zircon material (blue, **Figure 3**); partially metamict material reflecting a mixture of a glassy phase and a zircon phase (green, **Figure 3**); and amorphous $ZrSiO_4$ glass containing no indication of zircon structure (red, **Figure 3**). Additionally, the peak near 1008 cm^{-1} (i.e. the B_{1g}, $\nu_3(SiO4)$ band) was fitted for the spectra from the intact zircon and more metamict $ZrSiO_4$ phase in **Figure 3C** to get FWHM values. Intact zircon material had a FWHM of 7.8 ± 0.2 cm^{-1} while the metamict material had a 15.4 ± 1.8 cm^{-1}. This increased value demonstrates the broadening of the Raman spectral band in more metamict $ZrSiO_4$ material.

Reidite and zircon EBSD investigations

Microstructural EBSD analysis of grain A (the bright phase in the upper right side of **Figure 1a**) reveals that it is composed almost entirely of reidite (**Figure 4**). Two sets of {112} twinning planes disoriented 70° from <110> can be observed in this image. The {112} twins have been previously characterized in experimentally shock-produced reidite by transmission electron microscopy (TEM) (Leroux et al., 1999). The EBSD analyses of other experimentally shocked grains show variable mixtures of zircon and reidite such as the intergrown lamellae of zircon and reidite identified in **Figure 5**. A lift-out of the grain in **Figure 5** was taken by focused ion beam (FIB) and the FIB section was analyzed via transmission Kikuchi diffraction (TKD) (**Figure 6**). The interlocking lamellae of zircon and reidite, and {112} twin planes within the reidite are consistent with results from Leroux et al. (1999).

U-Pb geochronology

Uranium-lead isotopic analyses were conducted on a portion of the unshocked starting zircon grain and on a portion of the post-shock experiment shocked reidite material first via LA-ICP-MS, which suggested little variation between the unshocked zircon and the post-shock reidite, and then via SIMS. The average $^{207}Pb/^{206}Pb$ age of 16 LA-ICP-MS spots laid out in a vertical transverse across the unshocked starting zircon is 1067 ± 8.7 Ma (2 s.e.) with a ratio of $7.50\times10^{-2} \pm 5.2\times10^{-3}$ (2 s.e.). Only one laser analysis was placed on large reidite grain to conserve as much of the grain for future study and SIMS analyses. The LA-ICP-MS spot on the reidite sample yields a $^{207}Pb/^{206}Pb$ age of 1082 ± 42 Ma and ratio of $7.55\times10^{-2} \pm 1.6\times10^{-3}$. The Pb ratios, ages and Pb/U ratios for the unshocked zircon material and the post-shock reidite grain from both SIMS and LA-ICP-MS analyses are listed in **Table 1**.

Guided by the Raman map, the SIMS analyses of unshocked zircon were targeted on either intact zircon regions, or fully metamict $ZrSiO_4$ regions. The average isotope ratios of the unshocked intact zircon (n=10) yield $^{207}Pb/^{235}U = 1.84 \pm 4.1\times10^{-2}$ (2 s.e.) (1061 ± 15 Ma), $^{206}Pb/^{238}U = 1.8\times10^{-1} \pm 2.7\times10^{-3}$ (1069 ± 14 Ma) and $^{207}Pb/^{206}Pb = 7.42\times10^{-2} \pm 1.2\times10^{-3}$ (1046 ± 33 Ma). Spots acquired on metamict regions (n=6) yield $^{207}Pb/^{235}U = 1.81 \pm 4.5\times10^{-2}$ (1047 ± 16 Ma), $^{206}Pb/^{238}U$ of $1.76\times10^{-1} \pm 7.9\times10^{-3}$ (1043 ± 21 Ma), and $^{207}Pb/^{206}Pb = 7.5\times10^{-2} \pm 3.7\times10^{-4}$

(1055±21 Ma). Since the average isotopic ratios for intact zircon and the starting metamict regions overlap within 2 s.e. for the corresponding measurement averages, this is evidence that the metamict regions had similar U-Pb and Pb-Pb ratios to the intact zircon regions. This is important since we do not have a direct way of detecting if the post-shock experiment reidite was derived from a non-metamict zircon region or metamict $ZrSiO_4$ region. The s.d. for the metamict $ZrSiO_4$ region is higher than for the intact zircon regions indicating higher variability of U/Pb content in this region.

The SIMS analyses of the reidite spots (n=10) have $^{207}Pb/^{235}U = 1.81 \pm 5.4\times10^{-2}$ (1050 ± 20 Ma), $^{206}Pb/^{238}U = 1.79\times10^{-1} \pm 4.9\times10^{-3}$ (1061 ± 16 Ma), and radiogenic $^{207}Pb/^{206}Pb = 7.4\times10^{-2} \pm 1.8\times10^{-3}$ (1028 ± 50 Ma). These U-Pb and Pb-Pb average ratios for reidite all overlap within 2 s.e. for the intact zircon regions and the metamict $ZrSiO_4$ regions in the starting material. The reidite is slightly lower in U content (62 ppm) than the unshocked intact zircon (101 ppm) but this could be attributed to variations in U abundance in the $ZrSiO_4$ starting material. The concordia age for the SIMS analyses of the unshocked intact zircon is 1063±6.3 Ma (**Figure 7a**). The SIMS analyses from the unshocked metamict $ZrSiO_4$ are discordant (**Figure 7b**) and the concordia age for the reidite analyses from SIMS is 1053±20 Ma (**Figure 7c**). The concordia plot for reidite measurements (**Figure 7c**) shows larger error ellipses when compared with those from the unshocked intact zircon (**Figure 7a**). These are compared together in the same panel (**Figure 7d)** where it appears that the reidite measurements could have a slight tendency towards lower $^{206}Pb/^{238}U$ and $^{207}Pb/^{235}U$ values than the measurements from the intact zircon although statistical tests indicated this unlikely to be significant. The precise locations for the SIMS and LA-ICP-MS analyses on the reidite grain (grain A) and their $^{207}Pb/^{206}Pb$ and $^{206}Pb/^{238}U$ ages are shown in

Figure 8. These ages vary from a low 936±96 Ma to a high of 1199±53 Ma. Ages from both ends of these ranges can be found at adjacent spots.

Pb isotope measurements of feldspar

Turning our attention to Pb contamination and feldspar, **Table 2** presents LA-ICP-MS and SIMS data for the unshocked sanidine (multi-collector LA-ICP-MS; Simon et al., 2007), compared to our data from the shocked $KAlSi_3O_8$. The shocked $KAlSi_3O_8$ analyzed by SIMS yields $^{207}Pb/^{206}Pb = 8.18\times10^{-1} \pm 6.4\times10^{-3}$ (2 s.e.) whereas the unshocked sanidine from Simon et al. (2007) has a $^{207}Pb/^{206}Pb = 0.81813\pm 1.2\times10^{-5}$. The $^{208}Pb/^{206}Pb$ of the shocked material is $2.035 \pm 4.88\times10^{-2}$ while the unshocked sanidine (Simon et al., 2007) yields a $^{208}Pb/^{206}Pb$ ratio of $2.0303 \pm 2.5\times10^{-5}$. Ratios of radiogenic Pb compared to ^{204}Pb as analyzed by SIMS for unshocked intact zircon, metamict $ZrSiO_4$, post-experiment reidite, and shocked $KAlSi_3O_8$ are presented in **Table 3**. Common Pb results for shocked $KAlSi_3O_8$ are based on four SIMS analyses show average Pb-Pb ratios of $^{206}Pb/^{204}Pb = 1.9\times10^{1} \pm 3.2\times10^{-1}$, $^{207}Pb/^{204}Pb = 1.5\times10^{1} \pm 2.6\times10^{-1}$, $^{208}Pb/^{204}Pb$ of $3.8\times10^{1} \pm 6.4\times10^{-1}$ and $^{207}Pb/^{206}Pb = 8.18\times10^{-1} \pm 6.4\times10^{-3}$ and a $^{208}Pb/^{206}Pb = 2.035 \pm 4.9\times10^{-2}$. The $^{208}Pb/^{206}Pb$ and $^{207}Pb/^{206}Pb$ ratios from the Simon et al. (2007) analyses are indistinguishable from the same ratios derived for shocked $KAlSi_3O_8$ from SIMS. So, the Pb ratios between the unshocked sanidine and the shocked $KAlSi_3O_8$ were not changed by the shock experiment within the precision of our analyses.

Shock experiment simulation by iSALE2D modeling

We present three still-frame illustrations for pressure from an iSALE2D simulation of the experiment with conditions and dimensions of the target modeled after those used in the flat-plate experiment (**Figure 9a)**. A temperature version of **Figure 9a** and animations of **Figure 9b** and **Figure 9c** are in the SOM. The average of highest pressures reached for all the tracers in the simulation was 34 GPa while the average of the highest tracer temperatures reached in the simulation was ~1000 °C. The simulation shows pressure waves passing through that start at each end of the sample well and approach the center for a few timesteps. They appear around t=1.0 µs and have left the sample well by ~t=1.6 µs. The peak value that the *P-T* tracers experienced in the simulation is plotted in **Figure 10** where they are shown with x-y coordinates equivalent to their location at simulation start.

Discussion

Zircon to reidite transformation mechanism

The transformation mechanism of zircon to reidite is not fully understood, yet this is needed to provide clear constraints on the *P-T* conditions experienced from the shock event (Timms et al., 2017). The related microstructures allow insight into the transformation mechanisms, but there has been debate on whether this transformation occurs via a displacive (i.e. martensitic), or reconstructive method, or instead is a two-step process involving both types of mechanisms (e.g. Stangarone et al., 2019). In a displacive transformation, the phase transition occurs as a result of distorting the symmetry of the crystal structure. As a subset of displacive transformations, a martensitic (shear-dominated) displacive transformation has been proposed as mechanism for forming reidite (Leroux et al., 1999). For a reconstructive transition, the phases are not necessarily related by symmetry, as energy is also used for breaking or forming chemical bonds when transitioning to the new structure. The reconstructive hypothesis for formation of reidite is favored in Marqués et al. (2008). Since the transformation mechanism could also be a multi-step process, this could entail a transition to an intermediary phase via a displacive mechanism, and then completion of the transition to reidite reconstructively (Stangarone et al., 2019). During shock-loading the transition from zircon to reidite happens very quickly (<1 μs) (Kusaba et al., 1986) so a displacive mechanism may be a more favorable hypothesis than one that happens reconstructively. The crystallinity of the zircon structure before shock is another variable in the transformation of zircon to reidite. Erickson et al. (2017) investigated several zircon-bearing clasts from the Ries impact structure and found that both lamellar reidite and granular reidite were generated by this impact event. These two types suggest that multiple transformation pathways from zircon to reidite exist with displacive mechanisms being likely for lamellar impact generated reidite and a reconstructive transformation likely for granular reidite. One interesting sample is grain C which is composed of interlocking reidite and zircon lamellae (**Figure 5**).

We interpret our reidite as generated by a displacive mechanism operating on a mostly crystalline zircon domain. Evidence supporting a displacive transformation to reidite are the {112} twins, which likely formed as transformation twins minimizing the strain energy between the reidite and host zircon crystal structures. Although given the metamict regions found in the starting material, the two-step process of transition could also be favored here (cf. Stangarone et al. 2019). Reidite places a constraint on the temperature of the experiment. Immediately post shock, the temperature in the region of the reidite probably did not exceed 1200 °C (1473 K) for an appreciable length of time since reidite at that temperature (although at 1 atm) would have transitioned back to zircon (Kusaba et al., 1985). Intergrowths of reidite, like seen for grain C, have been identified in natural material from Ries crater that have experienced certain levels of shock (Wittman et al., 2006).

The iSALE2D simulation shows pressure waves carrying a pressure greater than 35 GPa **(Figure 9b)** that briefly transect the sample, which could be interpreted as excess pressure due to pore collapse because of the granular nature of sample. This could lead to localized regions of higher pressure and temperatures responsible for reidite in our post-shock material. The presented data suggests that many regions reached peak pressures surpassing 30 GPa and that while some regions of the sample experienced temperatures beyond 1200 °C, much of the sample saw peak temperatures between 800 and 1200 °C which is below the 1 atm reidite to zircon reversion temperature. Therefore, the simulations are consistent with the presence of the reidite observed in the post-shock experiment mineralogy.

Limited remobilization of Pb in the zircon and reidite

While the SIMS concordia age for the shocked reidite is 1053 ± 20 Ma and the unshocked intact zircon concordia age is 1063 ± 6.3 Ma, these values are not significantly different enough to indicate that the mineral transformation mechanism imparted a difference on the isotopic ages. Additionally, the similarity of the Pb isotopic data between the zircon and the reidite suggests that the shock loading process did not significantly alter the Pb content. However, it should be noted that the matrix effects between SIMS analyses of reidite and geochronology

DOI: https://doi.org/10.2138/am-2022-8604. http://www.minsocam.org/

zircon standards are unknown. Reidite is 10% denser than zircon but the similarity of the results between the two phases suggests that any matrix effects on the SIMS analyses between analyses of the two minerals are insignificant. Measurements of Pb-Pb isotope ratios are unlikely to be affected by matrix effects during SIMS analysis due to the small relative mass differences among the isotopes, leading to the nearly universal use of uncorrected measured $^{207}Pb/^{206}Pb$ for age calculation (e.g., Sequeira et al., 2020). Increased s.e. and sample s.d. on the reidite U-Pb and Pb-Pb age and ratio measurements compared to the intact zircon indicate only limited mobilization of Pb. The increased scatter on the reidite data could be due to the fact that the reidite domain has lower U content than the intact zircon. When SIMS data is averaged and the Pb-Pb ratios and U-Pb ages compared between the reidite and intact zircon, the reidite Pb-Pb ratio averages are consistently lower than the same average from the intact zircon. The same is also true when the reidite U-Pb ages are compared to the same average ages of the intact zircon measurements. Even so, for the both the Pb-Pb ratios and the U-Pb ages, the average values in the reidite are not younger or less than the same average value in intact zircon by more than 2%. Regardless of matrix effects, the similarity of our $^{207}Pb/^{206}Pb$ ages between zircon and reidite suggest that potential remobilization of Pb by the shock experiment or mineral transformation mechanism was limited at best and that there was no detectable ^{207}Pb or ^{206}Pb input from the feldspar. Therefore, our results support the conclusions from Deutsch and Schärer (1990) that at moderate levels, shock alone is not responsible for Pb mobilization within zircon grains from impact craters. If this is the case, then the U-Pb system may still generally preserve the original crystallization age after a moderate shock event unless significant post-shock heating occurs.

DOI: https://doi.org/10.2138/am-2022-8604. http://www.minsocam.org/

The possibility of Pb remobilization was further analyzed using statistical methods. While 10 datapoints from the unshocked intact zircon and 10 datapoints from the post-shock experiment reidite is a limited sampling to build a graphical normality test, a Shapiro-Wilkes test returned $p>0.05$ for the $^{207}Pb/^{206}Pb$, $^{207}Pb/^{235}U$, $^{206}Pb/^{238}U$ ages and ratios for both the unshocked intact zircon and the post-shock reidite, indicating that the datasets could be normally distributed. The $^{207}Pb/^{206}Pb$, $^{207}Pb/^{235}U$, $^{206}Pb/^{238}U$ ages and ratios between the unshocked intact zircon and post-shock reidite were also compared with a student's t-test, assuming unequal variance, which returned $p>0.05$ for all age and ratios. These results indicate that the levels of detected variability in the U-Pb content and ages of the reidite from the unshocked intact zircon are unlikely to be significant. This is also evidence that the transformation to reidite does not have significant effects on U-Pb content of the grain, supportive of a displacive mineral transformation mechanism in this experiment. The matching $^{208}Pb/^{206}Pb$ and $^{207}Pb/^{206}Pb$ ratios between the unshocked sanidine and the post-shock experiment sanidine suggest that the geochronology was not disturbed for this material either.

Implications

Results from our LA-ICP-MS and SIMS analyses indicate that the shock-loading experiment had only a limited effect on the age retention of any of the U-Pb geochronometers. When average SIMS analyses of the reidite are compared with average analyses of the intact zircon, while consistently lower, they differ by <2% for the main Pb-Pb and U-Pb ratios and ages. Therefore, our results support the conclusions of Deutsch and Schärer (1990) wherein they experimentally shocked zircon and determined that shock alone could not disturb the U-Pb system. Our analysis implies that the zircon to reidite transition may not notably affect the U-Pb ratios and that the use of reidite to date pre-impact terrain could be possible. Restated, geochronology conducted on reidite does not date the impact event.

The microstructural EBSD data provides good evidence of {112} twinning planes in the recovered reidite which is an additional confirmation of the Leroux et al., (1999) results. Our iSALE2D simulations suggest that many tracers experienced peak pressures >30 GPa yet that for many tracers, peak temperatures were around 800-1200 °C, consistent with the presence of reidite in our post-shock material. The match between our simulation and our post-experiment mineralogy indicates that hydrocode simulations (like iSALE) are useful for calculating temperatures experienced in flat-plate accelerator experiments along with providing insight into the experienced pressure when granular or porous material is being shocked.

Thanks and acknowledgements

We are grateful to Jacobs, the JETS contract, NASA ARES, University of Houston and University of Alabama. This project was partially supported by the Earth's First Origins NASA grant 80NSSC19M0069, 80NSSC22K0107, and NASA Planetary Science funding, NASA Solar System Workings grant 80NSSC20K1039, and by NSF EAR-2102143. Many thanks are due to Roland Montes and Frank Cardenas for assistance with the mechanics and gunning of the shot and Mark Cintala for input on gunning the shot. This project benefitted from fruitful discussions with Fred Hörz. Thanks are due to Zia Rahman for FIB liftout of material for transmission-Kikuchi-diffraction EBSD at NASA JSC. The assistance of Loan Le with spot Raman analyses was beneficial. The assistance of Minako Righter with LA-ICP-MS at the University of Houston was valuable. Grain sorting and grain mounting was done by Martha Miller at the University of Rochester and this project greatly benefitted from these efforts. We appreciate Rich Martens sample preparation assistance at the University of Alabama. Thanks for laboratory assistance are due to Nicole Haney, Rick Roland, Kathleen Vander Kaaden at Johnson Space Center and Wriju Chowdhury at the University of Rochester. We are grateful to Jay Thomas for assistance with additional Raman analyses during revisions at Syracuse University. For the impact simulations using the iSALE2D software, we gratefully acknowledge the developers of iSALE-2D, including Gareth Collins, Kai Wünnemann, Dirk Elbeshausen, Tom Davison, Boris Ivanov and Jay Melosh. The ion microprobe laboratory at UCLA is partially funded by a grant from NSF-EAR's Instrumentation and Facilities Program (1734856).

References

Akaogi, M., Hashimoto, S., and Kojitani, H. (2018). Thermodynamic properties of $ZrSiO_4$ zircon and reidite and of cotunnite-type ZrO_2 with application to high-pressure high-temperature phase relations in $ZrSiO_4$. Physics of the Earth and Planetary Interiors, 281, 1-7.

Alvarez, L.W., Alvarez, W., Asaro, F., and Michel, H.V., (1980) Extraterrestrial Cause for the Cretaceous-Tertiary Extinction. Science, 208(4448), 1095-1108

Amsden, A., Ruppel, H., and Hirt, C. (1980). SALE: A simplified ALE computer program for fluid flow at all speeds. Los Alamos National Laboratories Report, LA-8095:101p. Los Alamos, New Mexico: LANL

Bellucci, J.J., Nemchin, A.A., Whitehouse, M.J., Humayun, M., Hewins, R., Zanda, B. (2015) Pb-isotopic evidence for an early, enriched crust on Mars, Earth and Planetary Science Letters 410, 34-41.

Bellucci, J., Whitehouse, M., Nemchin, A., Snape, J., Pidgeon, R., Grange, M., Reddy, S.M. and Timms, N. (2016). A scanning ion imaging investigation into the micron-scale U-Pb systematics in a complex lunar zircon. Chemical Geology, 438, 112–122.

Cavosie, A.J., Biren, M.B., Hodges, K.V. Wartho J., Horton J.W. Jr., and Koeberl C. (2021) Dendritic reidite from the Chesapeake Bay impact horizon, Ocean Drilling Program Site 1073 (offshore northeastern USA): A fingerprint of distal ejecta?: Geology, v. 49, p. 201–205

Cavosie, A. J., Erickson, T. M., and Timms, N. E. (2015). Nanoscale records of ancient shock deformation: Reidite ($ZrSiO_4$) in sandstone at the Ordovician Rock Elm impact crater. Geology, 43(4), 315–318.

Cavosie, A. J., Erickson, T. M., Timms, N. E., Reddy, S.M., Talavera, C., Montalvo, S.D., Pincus, M.R., Gibbon, R.J., and Moser, D. (2016) A terrestrial perspective on using ex situ shocked zircons to date lunar impacts. Geology, 43(11), 999–1002.

Chen, M., Yin, F., Li, X., Xie, X., Xiao, W., and Tan, D. (2013). Natural occurrence of reidite in the Xiuyan crater of China. Meteoritics and Planetary Science, 48(5), 796–805.

Collins, G. S., Melosh, H. J., and Ivanov, B. A. (2004). Modeling damage and deformation in impact simulations. Meteoritics and Planetary Science, 39, 217-231.

Cox, M. A., Cavosie, A. J., Bland, P. A., Miljković, K., and Wingate, M. T. (2018). Microstructural dynamics of central uplifts: Reidite offset by zircon twins at the Woodleigh impact structure, Australia. Geology, 46(11), 983-986.

Crow, C. A., Mckeegan, K. D., and Moser, D. E. (2017). Coordinated U–Pb geochronology, trace element, Ti-in-zircon thermometry and microstructural analysis of Apollo zircons. Geochimica et Cosmochimica Acta, 202, 264–284.

Crow, C. A., Moser, D. E. and Mckeegan, K. D. (2019). Shock metamorphic history of >4Ga Apollo 14 and 15 zircons. Meteoritics and Planetary Science, 54(1), 181–201.

Crowley, J.L., Schoene, B., and Bowring, S.A. (2007). U-Pb dating of zircon in the Bishop Tuff at the millennial scale. Geology 35(12), 1123-1126

Deutsch, A., and Schärer, U. (1990). Isotope systematics and shock-wave metamorphism: I. U-Pb in zircon, titanite and monazite, shocked experimentally up to 59 GPa. Geochimica et Cosmochimica Acta, 54(12), 3427-3434.

Erickson, T. M., Cavosie, A. J., Moser, D. E., Barker, I. R., and Radovan, H. A. (2013). Correlating planar microstructures in shocked zircon from the Vredefort Dome at multiple scales: Crystallographic modeling, external and internal imaging, and EBSD structural analysis. American Mineralogist, 98(1), 53–65.

Erickson, T. M., Pearce, M. A., Reddy, S. M., Timms, N. E., Cavosie, A. J., Bourdet, J., Rickard, W.D.A., and Nemchin, A. A. (2017). Microstructural constraints on the mechanisms of the transformation to reidite in naturally shocked zircon. Contributions to Mineralogy and Petrology, 172(6).

Gibbons, R.V., and Ahrens, T.J. (1971). Shock Metamorphism of Silicate Glasses. Journal of Geophysical Research, 76 (23), 5489-5498

Gibbons, R.V., (1974) Experimental Effects of Shock Pressure on Materials of Geological and Geophysical Interest, Ph.D. Thesis, California Institute of Technology

Glass, B., and Liu, S. (2001). Discovery of high-pressure $ZrSiO_4$ polymorph in naturally occurring shock-metamorphosed zircons. Geology, 29(4), 371.

Glass, B. P., Liu, S., and Leavens, P. B. (2002). Reidite: An impact-produced high-pressure polymorph of zircon found in marine sediments. American Mineralogist, 87(4), 562–565.

Gleason, G., Sunny, S., Sadeh, S., Yu, H., and Malik, A. (2020) Eulerian Modeling of Plasma-Pressure Driven Laser Impact Weld Processes. 48th SME North American Manufacturing Research Conference, NAMRC 48 (Cancelled due to COVID-19), Procedia Manufacturing, 48, 204-214

Gucsik, A., Koeberl, C., Brandstätter, F., Reimold, W. U., and Libowitzky, E. (2002). Cathodoluminescence, electron microscopy, and Raman spectroscopy of experimentally shock-metamorphosed zircon. Earth and Planetary Science Letters, 202(2), 495–509.

Gucsik, A., Koeberl, C., Brandstätter, F., Libowitzky, E., and Reimold, W. U. (2004a). Cathodoluminescence, Electron Microscopy, and Raman Spectroscopy of Experimentally Shock Metamorphosed Zircon Crystals and Naturally Shocked Zircon from the Ries Impact Crater. Cratering in Marine Environments and on Ice Impact Studies, 281-322.

Gucsik, A., Zhang, M., Koeberl, C., Salje, E. K., Redfern, S. A., and Pruneda, J. M. (2004b). Infrared and Raman spectra of ZrSiO4 experimentally shocked at high pressures. Mineralogical Magazine, 68(5), 801-811.

Gucsik, A. (2007) Micro-Raman Spectroscopy of Reidite as an Impact-Induced High Pressure Polymorph of Zircon: Experimental Investigation and Attempt to Application, Acta Mineralogica-Petrographica, 47, 17-24

Grieve, R.A.F., Langenhorst, F., and Stoffler, D. (1996). Shock metamorphism of quartz in nature and experiment: II. Significance in geoscience. Meteoritics and Planetary Science, 31, 6-35

Hapke, B., and Sato, H. (2016). The porosity of the upper lunar regolith. Icarus, 273, 75-83

Hildebrand A.R., Penfield, G.T., Kring, D.A., Pilkington, M., Carmago Z., A., Jacobsen, S.B., and Boynton W.V. (1991) Chicxulub Crater: A possible Cretaceous/Tertiary boundary impact crater on the Yucatán Peninsula, Mexico Geology, 19 (9), 867–871.

Hopkins, M.D. and Mojzsis, S.J. (2015) A protracted timeline for lunar bombardment from mineral chemistry, Ti thermometry and U–Pb geochronology of Apollo 14 melt breccia zircons. Contributions to Mineralogy and Petrology, 169(30), 1-18.

Hopkins, M.D., Mojzsis, S.J., Bottke, W.F., and Abramov O. (2015) Micrometer-scale U–Pb age domains in eucrite zircons, impact re-setting, and the thermal history of the HED parent body. Icarus, 245, 367-378

Humayun, M., Nemchin, A., Zanda, B., Hewins, R. H., Grange, M., Kennedy, A., Lorand, J.-P., Göpel, C., Fieni, C., Pont, S., and Deldicque, D. (2013). Origin and age of the earliest Martian crust from meteorite NWA 7533. Nature, 503(7477), 513-516.

Ivanov, B. A., Deniem, D., and Neukum, G. (1997). Implementation of dynamic strength models into 2D hydrocodes: Applications for atmospheric breakup and impact cratering. International Journal of Impact Engineering, 20, 411-430.

Ireland, T.R., and Wlotzka, F., (1992) The oldest zircons in the solar system. Earth and Planetary Science Letters, 109(1-2), 1-10.

Kieffer, S.W., (1971), Shock Metamorphism of the Coconino Sandstone at Meteor Crater, Arizona. Journal of Geophysical Research 76(23), 5449-5473.

Knittle, E., Williams, Q., (1993). High-pressure Raman spectroscopy of $ZrSiO_4$: Observation of the zircon to scheelite transition at 300 K. American Mineralogist, 78, 245-252.

Krogh, T. E., Kamo, S. L., Sharpton, V. L., Marin, L. E., and Hildebrands, A. R. (1993). U–Pb ages of single shocked zircons linking distal K/T ejecta to the Chicxulub crater. Nature, 366(6457), 731–734.

Kusaba, K., Syono, Y., Kikuchi, M., and Fukuoka, K. (1985). Shock behavior of zircon: phase transition to scheelite structure and decomposition. Earth and Planetary Science Letters, 72(4), 433–439.

Kusaba, K., Yagi, T., Kikuchi, M., and Syono, Y. (1986). Structural considerations on the mechanism of the shock-induced zircon-scheelite transition in ZrSiO4. Journal of Physics and Chemistry of Solids, 47(7), 675–679

Leroux, H., Reimold, W., Koeberl, C., Hornemann, U., and Doukhan, J. (1999). Experimental shock deformation in zircon: A transmission electron microscopic study. Earth and Planetary Science Letters, 169(3-4), 291-301.

Leroux H., Jacob D., Marinova, M., Hewins, R.H., Zanda, B., Pont, S., Lorand, JP., and Humayun M. (2016) Exsolution and shock microstructures of igneous pyroxene clasts in the Northwest Africa 7533 Martian meteorite Meteoritics and Planetary Science, 51(5), 932–945

Liu, L.-G. (1979). High-pressure phase transformations in baddeleyite and zircon, with geophysical implications. Earth and Planetary Science Letters, 44(3), 390–396

Liu, Y., Ma, C., Beckett, J. R., Chen, Y., and Guan, Y. (2016). Rare-earth-element minerals in martian breccia meteorites NWA 7034 and 7533: Implications for fluid–rock interaction in the martian crust. Earth and Planetary Science Letters, 451, 251-262.

Ludwig, K.R. ,(2003) Isoplot 3.00: A geochronological toolkit for Microsoft Excel. Berkeley Geochronology Center Special Publication.

Malavergne, V., Guyot, F., Benzerara, K., Martinez, I. (2001) Description of new shock-induced phases in the Shergotty, Zagami, Nakhla and Chassigny meteorites. Meteoritics and Planetary Science, 36, 1297-1305

Mark, D. F., Renne, P. R., Dymock, R. C., Smith, V. C., Simon, J. I., Morgan, L. E., Staff, R.A., Ellis, B.S. and Pearce, N. J. (2017). High-precision 40Ar/39Ar dating of pleistocene tuffs and temporal anchoring of the Matuyama-Brunhes boundary. Quaternary Geochronology, 39, 1–23.

Marqués, M., Contreras-García, J., Flórez, M., and Recio, J. (2008). On the mechanism of the zircon-reidite pressure induced transformation. Journal of Physics and Chemistry of Solids, 69(9), 2277–2280.

Melosh, H. J., Ryan, E. V., and Asphaug, E. (1992). Dynamic fragmentation in impacts: Hydrocode simulation of laboratory impacts. Journal of Geophysical. Research, 97(E9), 14735-14759

Mernagh, T.P. (1991) Use of the laser Raman microprobe for discrimination amongst feldspar minerals. Journal of Raman Spectroscopy, 22, 453-457

Moser, D. E. (1997). Dating the shock wave and thermal imprint of the giant Vredefort impact, South Africa. Geology, 25(1), 7.

Moser, D. E., Cupelli, C. L., Barker, I. R., Flowers, R. M., Bowman, J. R., Wooden, J., and Hart, J. (2011). New zircon shock phenomena and their use for dating and reconstruction of large impact structures revealed by electron nanobeam (EBSD, CL, EDS) and isotopic U–Pb and (U–Th)/He analysis of the Vredefort dome Special Issue. Canadian Journal of Earth Sciences, 48(2), 117–139.

Moser, D. E., Chamberlain, K. R., Tait, K. T., Schmitt, A. K., Darling, J. R., Barker, I. R., and Hyde, B. C. (2013). Solving the Martian meteorite age conundrum using micro-baddeleyite and launch-generated zircon. Nature, 499(7459), 454–457.

Moser, D.E., Arcuri, G. A., Reinhard, D. A., White, L. F., Darling, J. R., Barker, I. R., Larson, D. J., Irving, A. J., McCubbin, F. M., Tait, K. T., Roszjar, J., Wittmann, A. and Davis C. (2019) Decline of giant impacts on Mars by 4.48 billion years ago and an early opportunity for habitability. Nature Geoscience, 12, 522–527

Nemchin, A., Timms, N., Pidgeon, R., Geisler, T., Reddy, S., and Meyer, C. (2009). Timing of crystallization of the lunar magma ocean constrained by the oldest zircon. Nature Geoscience, 2(2), 133–136.

Ono, S., Funakoshi, K., Nakajima, Y., Tange, Y., and Katsura, T. (2004). Phase transition of zircon at high P-T conditions. Contributions to Mineralogy and Petrology, 147(4), 505–509.

Ostertag, R. (1983). Shock experiments on feldspar crystals. Journal of Geophysical Research, 88(S01).

Pidgeon, R., Nemchin, A., Bronswijk, W. V., Geisler, T., Meyer, C., Compston, W., and Williams, I. (2007). Complex history of a zircon aggregate from lunar breccia 73235. Geochimica Et Cosmochimica Acta, 71(5), 1370–1381.

Rasmussen, C., Stockli D.F., Ross, C.H., Pickersgill, A., Gulick S.P., Schmieder M., Christeson G.L.,[a]Wittmann A., Kring D.A., Morgan J.V., and the IODP-ICDP Expedition 364 Science Party (2019). U-Pb memory behavior in Chicxulub's peak ring — Applying U-Pb depth profiling to shocked zircon. Chemical Geology, 525, 356-367.

Reid, A.F., and Ringwood, A.E. (1969). Newly observed high pressure transformations in Mn_3O_4, $CaAl_2O_4$, and $ZrSiO_4$. Earth and Planetary Science Letters, 6, 205–208

Reddy, S., Timms, N.E., Trimby, P., Kinny, P.D., Buchan, C., Blake, K. (2006). Crystal-plastic deformation of zircon: A defect in the assumption of chemical robustness. Geology, 34 (4), 257–260.

Reddy, S., Johnson, T., Fischer, S., Rickard, W., and Taylor, R. (2015). Precambrian reidite discovered in shocked zircon from the Stac Fada impactite, Scotland. Geology, 43(10), 899–902.

Reddy, S. M., Riessen, A. V., Saxey, D. W., Johnson, T. E., Rickard, W. D., Fougerouse, D., Fischer, S., Prosa, T.J., Rice, K.P., Reinhard, D.A., Chen, Y., and Olson, D. (2016). Mechanisms of deformation-induced trace element migration in zircon resolved by atom probe and correlative microscopy. Geochimica Et Cosmochimica Acta, 195, 158-170.

Roszjar, J., Whitehouse, M., Srinivasan, G., Mezger, K., Scherer, E., Orman, J. V., and Bischoff, A. (2016). Prolonged magmatism on 4 Vesta inferred from Hf–W analyses of eucrite zircon. Earth and Planetary Science Letters, 452, 216-226.

Sañudo-Wilhelmy, S. A., & Flegal, A. R. (1994). Temporal variations in lead concentrations and isotopic composition in the Southern California Bight. Geochimica et Cosmochimica Acta, 58(15), 3315-3320.

Schaal R. B. and Horz F. (1977) Shock metamorphism of lunar and terrestrial basalts. Proceedings of the 8th Lunar Science Conference, 1697-1729

Schaal, R.B., Hörz, F., Thompson, T.D., and Bauer, J.F. (1979) Shock Metamorphism of Granulated Lunar Basalt. Proceedings of the 10th Lunar and Planetary Science Conference., 2547-2571.

Schulte, P., Alegret, L., Arenillas, I., Arz, J.A., Barton, P.J., Bown, P.R., Bralower, T.J., Christeson, G.L., Claeys, P., Cockell, C.S., and others. (2010) The Chicxulub Asteroid Impact and Mass Extinction at the Cretaceous-Paleogene Boundary. Science, 327, 1214-1219

Sequeira, N., Mahato, S., Rahl, J.M., Sarkar, S., and Bhattacharya, A., (2020) The Anatomy and Origin of a Synconvergent Grenvillian-Age Metamorphic Core Complex, Chottanagpur Gneiss Complex, Eastern India, Lithosphere (1): 8833404.

Simon, J. I., Reid, M.R. (2005). The pace of rhyolite differentiation and storage in an 'archetypical' silicic magma system, Long Valley, California. Earth and Planetary Science Letters 235, 123-140.

Simon, J. I., Reid, M.R., and Young, E.D. (2007). Lead isotopes by LA-MC-ICPMS: Tracking the emergence of mantle signatures in an evolving silicic magma system. Geochimica Et Cosmochimica Acta,71(8), 2014-2035

Smit, J., and Hertogen, J. (1980) An extraterrestrial event at the Cretaceous–Tertiary boundary. Nature (London), 285(5762), 198-200

Stangarone, C., Angel, R. J., Prencipe, M., Mihailova, B., and Alvaro, M. (2019). New insights into the zircon-reidite phase transition. American Mineralogist, 104(6), 830–837.

Taylor, D. J., Mckeegan, K. D., and Harrison, T. M. (2009). Lu–Hf zircon evidence for rapid lunar differentiation. Earth and Planetary Science Letters, 279(3-4), 157–164

Timms, N. E., Kinny, P. D., and Reddy, S. M. (2006). Enhanced diffusion of Uranium and Thorium linked to crystal plasticity in zircon. Geochemical Transactions, 7(1).

Timms, N.E., Erickson, T. M., Pearce, M.A., Cavosie, A.J., Schmieder, M., Tohver, E., Reddy, S.M., Zanetti, M.R., Nemchin, A.A., and Wittmann, A. (2017a) A pressure-temperature phase diagram for zircon at extreme conditions. Earth-Science Reviews 165, 185-202.

Timms, N.E., Erickson, T.M., Zanetti M.R., Pearce M.A., Cayron C., Cavosie, A.J., Reddy, S.M., Wittmann A., and Carpenter P.K. (2017b) Cubic zirconia in >2370 °C impact melt records Earth's hottest crust. Earth and Planetary Science Letters, 477, 52-58

Trail, D., Barboni, M. and McKeegan, K.D. (2020) Evidence for diverse lunar melt compositions and mixing of the pre-3.9 Ga crust from zircon chemistry. Geochimica et Cosmochimica Acta 284, 173-195.

Westrenen, W. V., Frank, M. R., Hanchar, J. M., Fei, Y., Finch, R. J., and Zha, C. (2004). In situ determination of the compressibility of synthetic pure zircon (ZrSiO4) and the onset of the zircon-reidite phase transition. American Mineralogist, 89(1), 197-203.

White, L., Darling, J., Moser, D., Cayron, C., Barker, I., Dunlop, J., and Tait, K. (2018). Baddeleyite as a widespread and sensitive indicator of meteorite bombardment in planetary crusts. Geology, 46(8), 719–722.

Wiedenbeck, M., Allé, P., Corfu, F., Griffin, W.L., Meier, M., Oberli, F., Von Quadt, A., Roddick, J.C., and Spiegel, W., (1995) Three Natural Zircon Standards For U-Th-Pb, Lu-Hf, Trace Element And REE Analyses. Geostandards Newsletter, 19(1), 1-23

Wiedenbeck, M., Hanchar, J. M., Peck, W. H., Sylvester, P., Valley, J., Whitehouse, M., Kronz, A., Morishita, Y., Nasdala, L., Fiebig, J., and others (2004). Further Characterisation of the 91500 Zircon Crystal. Geostandards and Geoanalytical Research, 28(1), 9–39.

Wielicki, M.M., and Harrison, T.M., (2015) Zircon formation in impact melts: Complications for deciphering planetary impact histories. The Geological Society of America Special Paper 518, 127-134

Wittmann, A., Cavosie, A.J., Timms, N.E., Ferrière, L., Rae, A., Rasmussen, C., Ross, C., Stockli, D., Schmieder, M., Kring, D.A., Zhao, J., and others (2021) Shock impedance amplified impact deformation of zircon in granitic rocks from the Chicxulub impact crater, Earth and Planetary Science Letters, 575, 1-13

Wittmann, A., Kenkmann, T., Schmitt, R. T., and Stöffler, D. (2006). Shock-metamorphosed zircon in terrestrial impact craters. Meteoritics and Planetary Science, 41(3), 433–454.

Wünnemann, K., Collins, G., and Melosh, H. (2006). A strain-based porosity model for use in hydrocode simulations of impacts and implications for transient crater growth in porous targets. Icarus, 180, 514—527

Xing, W., Lin, Y., Zhang, C., Zhang, M., Hu, S., Hofmann, B. A., Sekine, T., Xiao, L., and Gu, L., (2020) Discovery of Reidite in the Lunar Meteorite Sayh al Uhaymir 169, Geophysical Research Letters, 47(21), 1-8

Zhang, M., Salje, E. K. H., Farnan, I., Graeme-Barber, A., Daniel, P., Ewing, R. C., Clark, A.M., and Leroux, H. (2000). Metamictization of zircon: Raman spectroscopic study. Journal of Physics: Condensed Matter, 12(8), 1915–1925.

Tables

Table 1

	n	$^{207}Pb/^{235}U$	$^{207}Pb/^{235}U$ 2 s.e.	$^{206}Pb/^{238}U$	$^{206}Pb/^{238}U$ 2 s.e.	$^{207}Pb/^{206}Pb$	$^{207}Pb/^{206}Pb$ 2 s.e.	$^{207}Pb/^{206}Pb$ Age (Ma) ±2 s.e.	$^{207}Pb/^{235}U$ Age (Ma) ±2 s.e.	$^{206}Pb/^{238}U$ Age (Ma) ±2 s.e.	U ppm ±2 s.e.	Th ppm ±2 s.e.
LA-ICP-MS												
Unshocked												
Zircon-Vertical Traverse Average	16	1.84	1.37×10^{-1}	1.78×10^{-1}	9.6×10^{-3}	7.50×10^{-2}	5.2×10^{-3}	1067 ± 8.7Ma	1060± 3.1 Ma	1057.4 ± 3.3 Ma	183 ±0.9	54 ±0.23
Shocked												
Reidite	1	1.86	5.5×10^{-2}	1.78×10^{-1}	4.1×10^{-3}	7.55×10^{-2}	1.6×10^{-3}	1082 ± 42 Ma	1065.3 ± 19.5 Ma	1058.0 ± 22.6 Ma	146 ±2.2	47 ±0.63
SIMS												
Unshocked												
Intact zircon	10	1.84	4.1×10^{-2}	1.8×10^{-1}	2.7×10^{-3}	7.42×10^{-2}	1.2×10^{-3}	1046 ±33	1061 ±15	1069 ±14	101 ±6.6	29 ±0.70
Metamict $ZrSiO_4$	6	1.81	4.5×10^{-2}	1.76×10^{-1}	7.9×10^{-3}	7.5×10^{-2}	7.6×10^{-4}	1055 ±21	1047 ±16	1043 ±21	2202 ±199	629 ±33
Shocked												
Reidite	10	1.81	5.4×	1.79	2.9	7.4	1.8	1028	1050	1061	62	20

			10^{-2}	$\times10^{-1}$	$\times10^{-3}$	$\times10^{-2}$	$\times10^{-3}$	±50	±20	±16	±5	±0.51

Table 2

	n	$^{207}Pb/^{206}Pb$	$^{207}Pb/^{206}Pb$ 2 s.e.	$^{208}Pb/^{206}Pb$	$^{208}Pb/^{206}Pb$ 2 s.e.
<u>Unshocked</u>					
Sanidine - Average from the LV51 multi-collector dataset from Simon et al. (2007)	11	8.18126×10^{-1}	1.2×10^{-5}	2.03031	2.5×10^{-5}
<u>Shocked</u>					
Sanidine - LA-ICP-MS spots	8	8.10×10^{-1}	2.8×10^{-2}	2.046	3.5×10^{-2}
Sanidine - SIMS analyses	4	8.18×10^{-1}	6.4×10^{-3}	2.035	4.9×10^{-2}

Table 3

	n	$^{206}Pb/^{204}Pb$	$^{206}Pb/^{204}Pb$ 2 s.e.	$^{207}Pb/^{204}Pb$	$^{207}Pb/^{204}Pb$ 2 s.e.	$^{208}Pb/^{204}Pb$	$^{208}Pb/^{204}Pb$ 2 s.e.
SIMS							
Unshocked							
Intact zircon	10	7.95×10^{3}	3.73×10^{3}	6.01×10^{2}	2.73×10^{2}	7.20×10^{2}	3.42×10^{2}
Metamict $ZrSiO_4$	8	5.19×10^{4}	1.77×10^{4}	3.89×10^{3}	1.32×10^{3}	3.16×10^{3}	1.02×10^{3}
Shocked							
Reidite	10	2.42×10^{3}	5.57×10^{2}	1.95×10^{2}	4.54×10^{1}	2.62×10^{2}	6.17×10^{1}
Sanidine	4	1.9×10^{1}	3.2×10^{-1}	1.5×10^{1}	2.6×10^{-1}	3.8×10^{1}	6.4×10^{-1}

Figures

Figure 1:

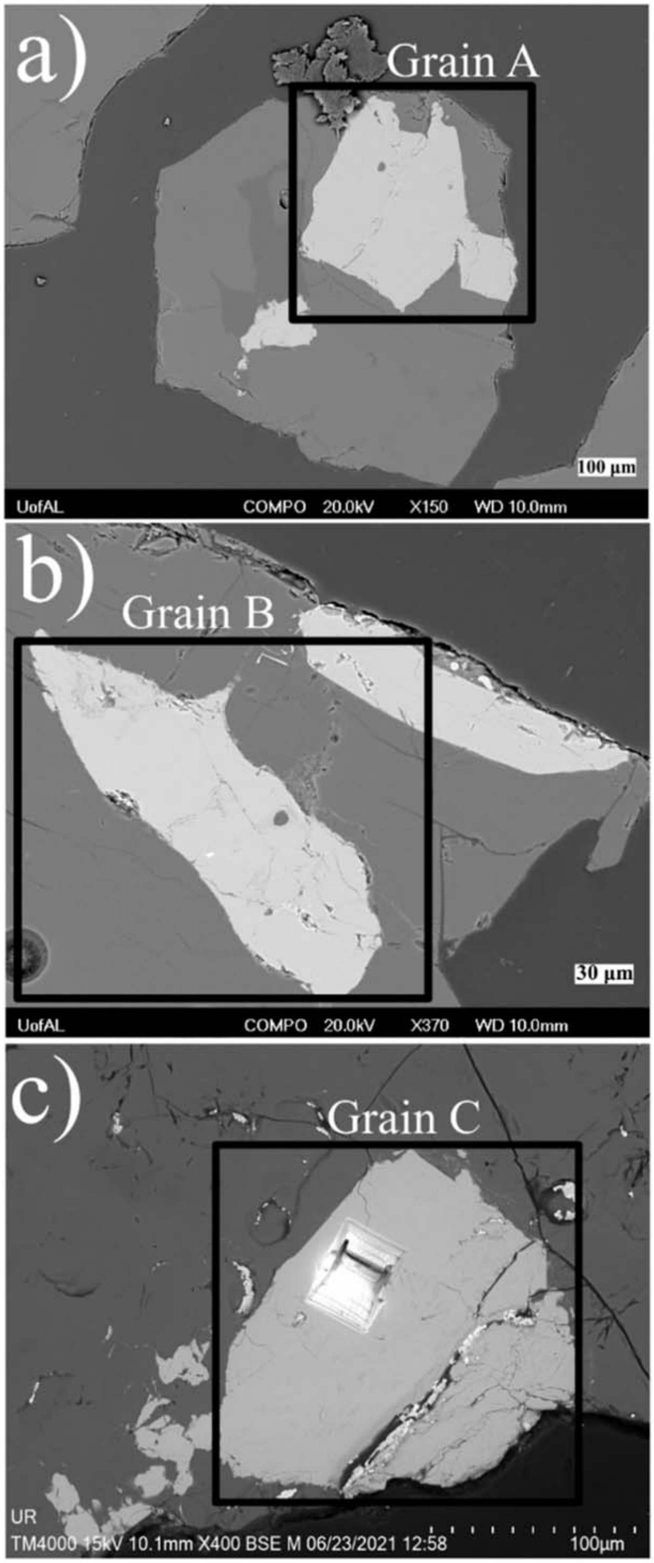

Figure 1, (a) BSE image of experimentally shocked zircon and sanidine with the large backscatter bright grain in the upper right referred to as grain A. This grain is mostly reidite as

This is the peer-reviewed, final accepted version for American Mineralogist, published by the Mineralogical Society of America.
The published version is subject to change. Cite as Authors (Year) Title. American Mineralogist, in press.
DOI: https://doi.org/10.2138/am-2022-8604. http://www.minsocam.org/

identified by EBSD and Raman analyses. **(b)** Experimentally shocked $ZrSiO_4$ referred to as grain B that is mostly amorphous. Multiple Raman spectra from this grain are presented in the **Figure S13** in the SOM to confirm its general lack of structure. **(c)** Experimentally shocked material (grain C). This grain showed evidence of both reidite and zircon lamellae being present. A FIB liftout was taken from grain C for later analysis which is why a section of the grain is carved out.

Figure 2:

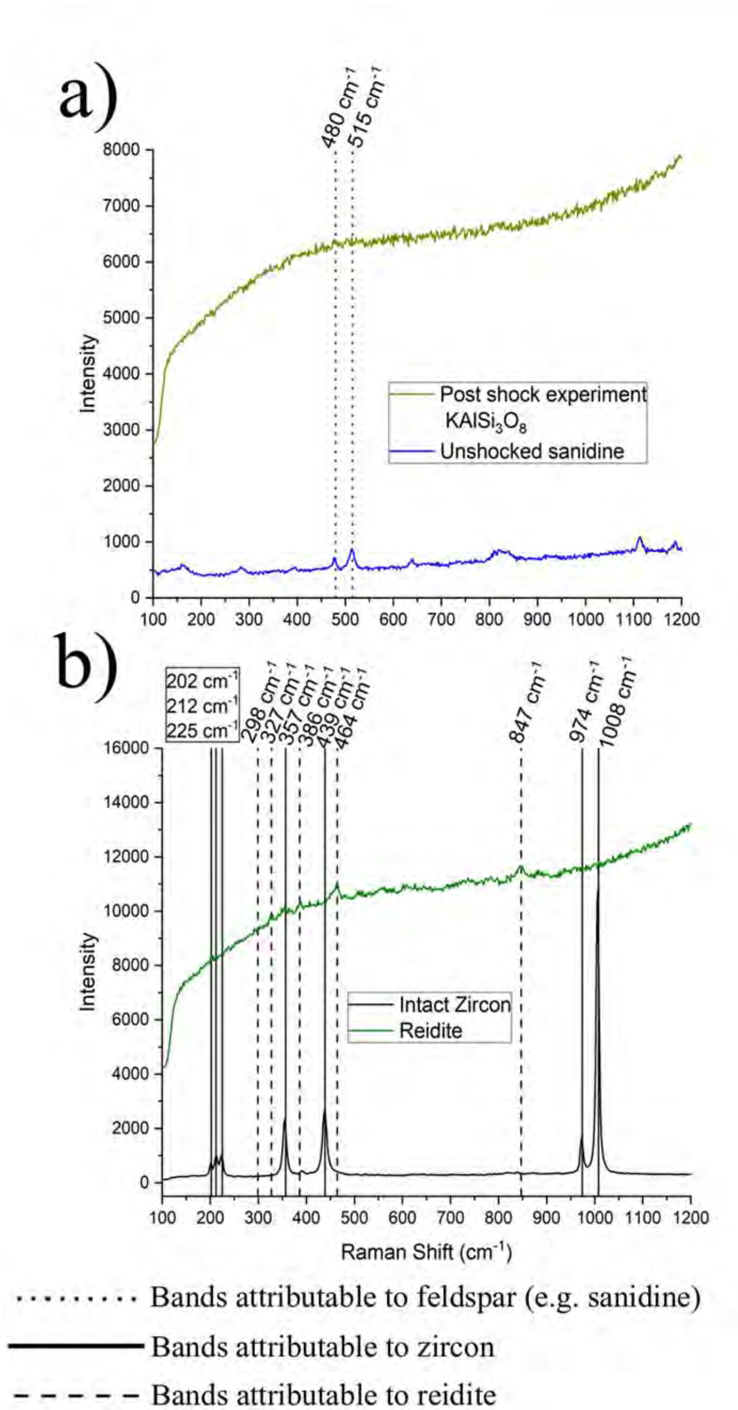

806

807 **Figure 2, (a)** Raman spectra of unshocked sanidine and the formerly sanidine material which has
808 become diaplectic $KAlSi_3O_8$ glass after the shock experiment. **3b)** $ZrSiO_4$ Raman spectra from
809 intact zircon material set aside before the shock experiment, and post-shock experiment material

found to be reidite. This material was determined to be primarily reidite by EBSD and the bands present in the Raman spectrum help confirm this result.

Figure 3:

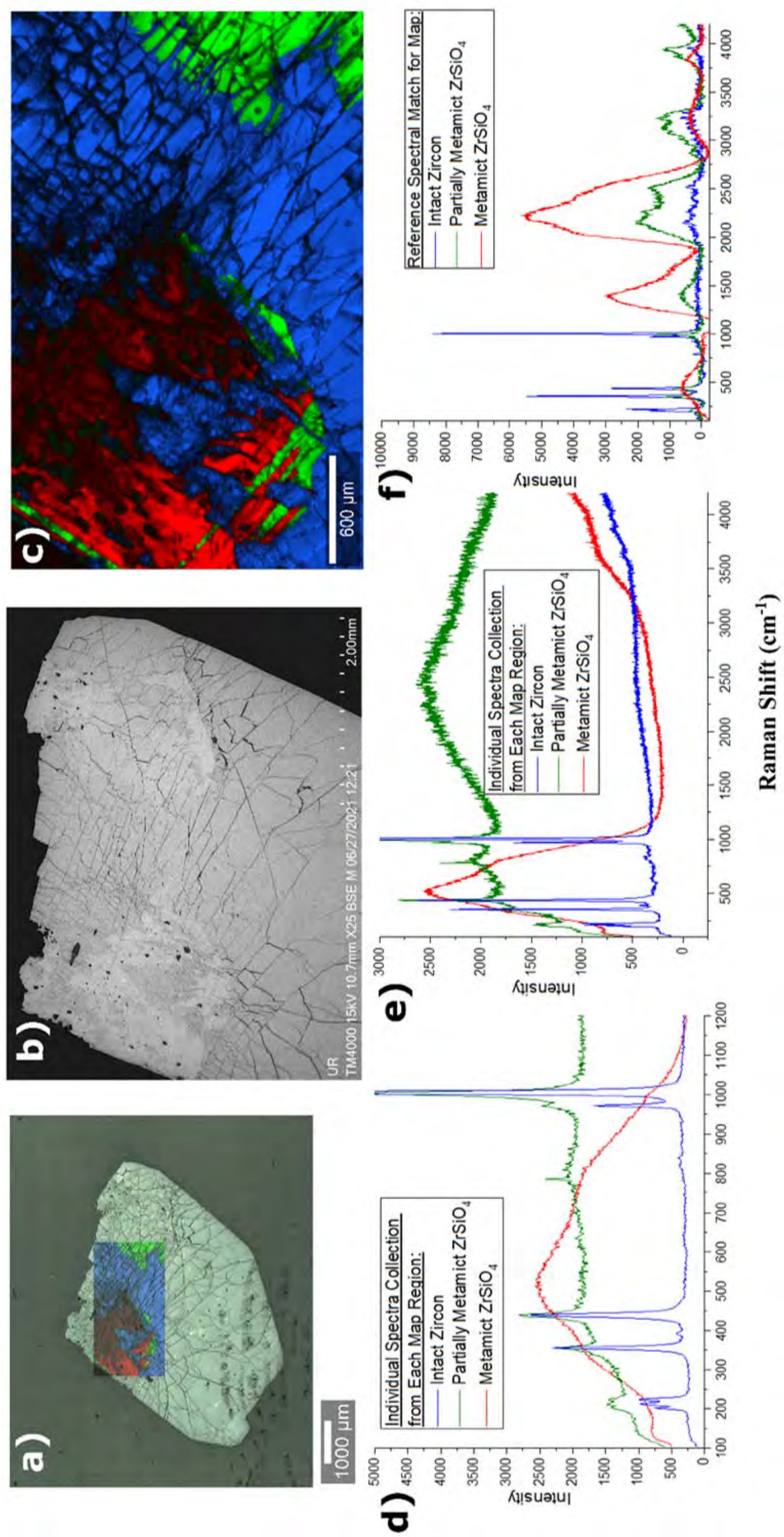
a)
1000 µm
b)
UR
TM4000 15kV 10.7mm X25 BSE M 06/27/2021 12:21
2.00mm
c)
600 µm
d)
Individual Spectra Collection from Each Map Region:
Intact Zircon
Partially Metamict ZrSiO4
Metamict ZrSiO4
Intensity
e)
Individual Spectra Collection from Each Map Region:
Intact Zircon
Partially Metamict ZrSiO4
Metamict ZrSiO4
Intensity
f)
Reference Spectral Match for Map:
Intact Zircon
Partially Metamict ZrSiO4
Metamict ZrSiO4
Intensity
Raman Shift (cm-1)

DOI: https://doi.org/10.2138/am-2022-8604. http://www.minsocam.org/

Figure 3. **(a)** An optical image with overlayed Raman map analyzed for a portion of the unshocked zircon grain with **(b)** BSE SEM image of the region and **(c)** the Raman map itself. Three regions are apparent from the Raman map. The map was generated via the WITec Basic Analysis feature which compares collected spectra to example spectra and assigns a fit score for each. In **(d)** individual spectra collected from these regions are shown to 1200 cm^{-1} while in **(e)** they are plotted to 4200 cm^{-1}. Then **(f)** shows the reference spectra matched to for generating the map.

DOI: https://doi.org/10.2138/am-2022-8604. http://www.minsocam.org/

868

869 **Figure 4:**

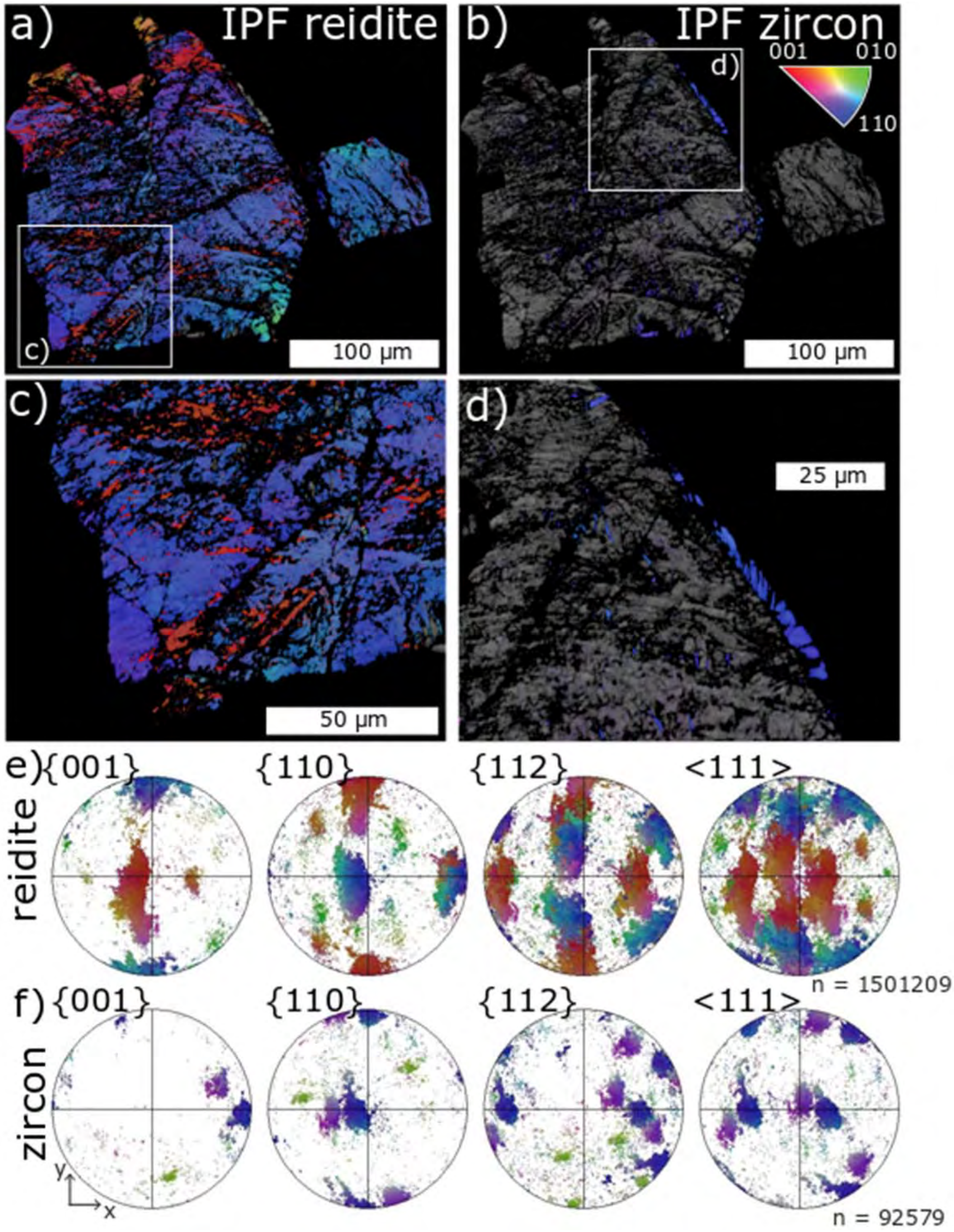

870

DOI: https://doi.org/10.2138/am-2022-8604. http://www.minsocam.org/

Figure 4. EBSD inverse pole figure color (z direction) maps of the material identified as grain A. This grain is a ~300 μm grain that is almost entirely composed of reidite. The boxes in **(a)** and **(b)** indicate particular regions of the grain that are shown in more detail in **(c)** and **(d)** respectively with **(d)** showing small amount of zircon on the northeast side of the grain. Pole figures for the EBSD map are **(e)** for reidite and **(f)** for zircon.

899 **Figure 5:**

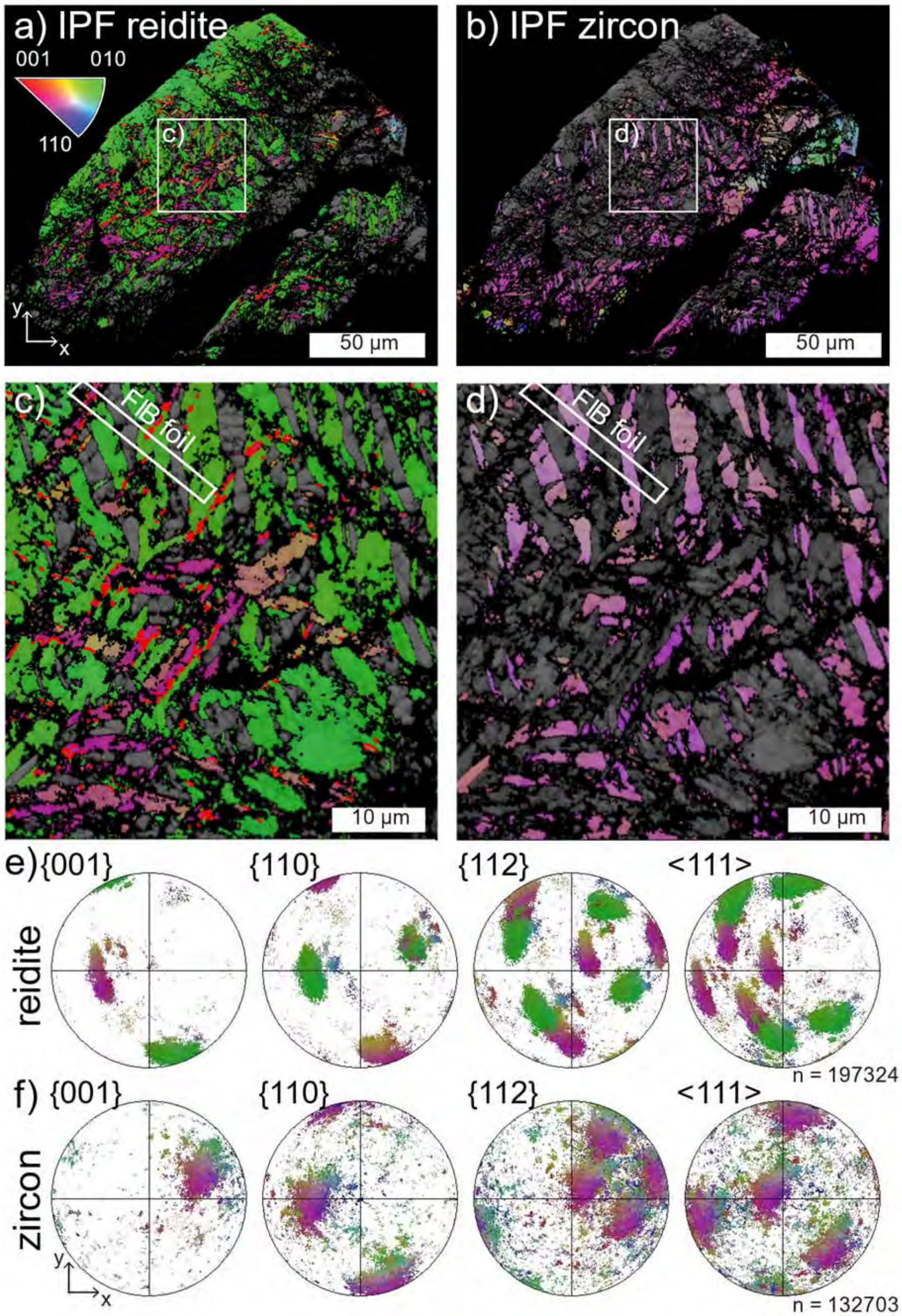

900

Figure 5. EBSD maps and pole figures of shocked zircon-reidite material (grain C). **(a)** Inverse pole figure (z direction) exhibiting a reidite domain about 50 to 100 μm. **(b)** Unlike the other reidite domain (i.e., grain A from **Figure 4a**), this one has several small lamellae of zircon running through it. **(c)** Close-up view of the grain with material indexed as reidite via EBSD. **(d)** The same region but showing the material indexed as zircon. Due to the intriguing nature of the intergrown reidite and zircon lamellae, this sample was targeted for FIB liftout of a section marked by the white box in **(c)** and **(d). (e)** Pole figures for reidite and **(f)** for zircon.

Figure 6:

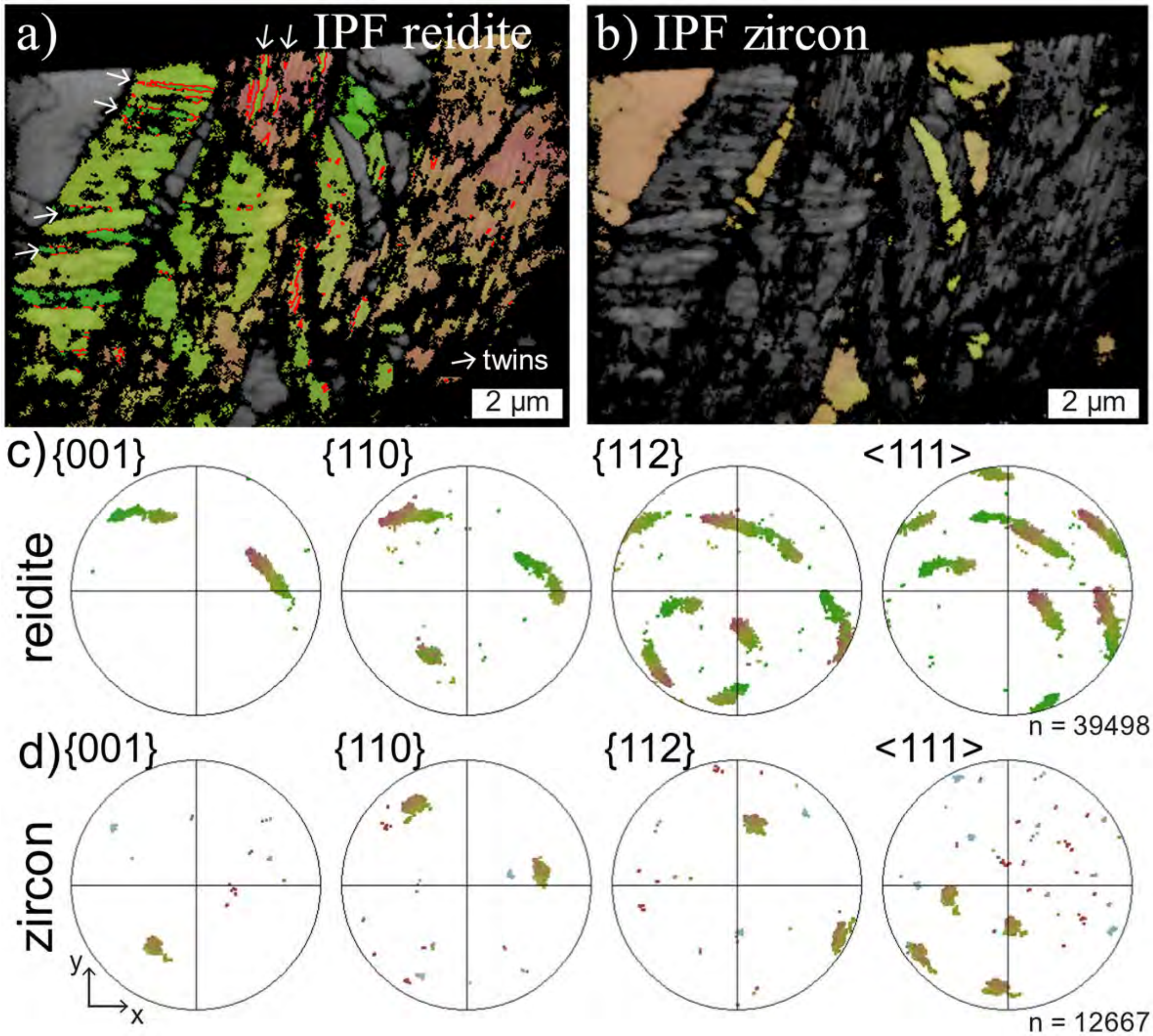

Figure 6. Transmission-EBSD figures on the FIB segment lifted out from the shocked product referred to as grain C. **(a)** Shows an inverse pole figure (z direction) map of material which indexed as reidite with major twins marked. **7(b)** Material which indexed as zircon. **(c)** The pole figures for reidite and **7(d)** for zircon.

Figure 7:

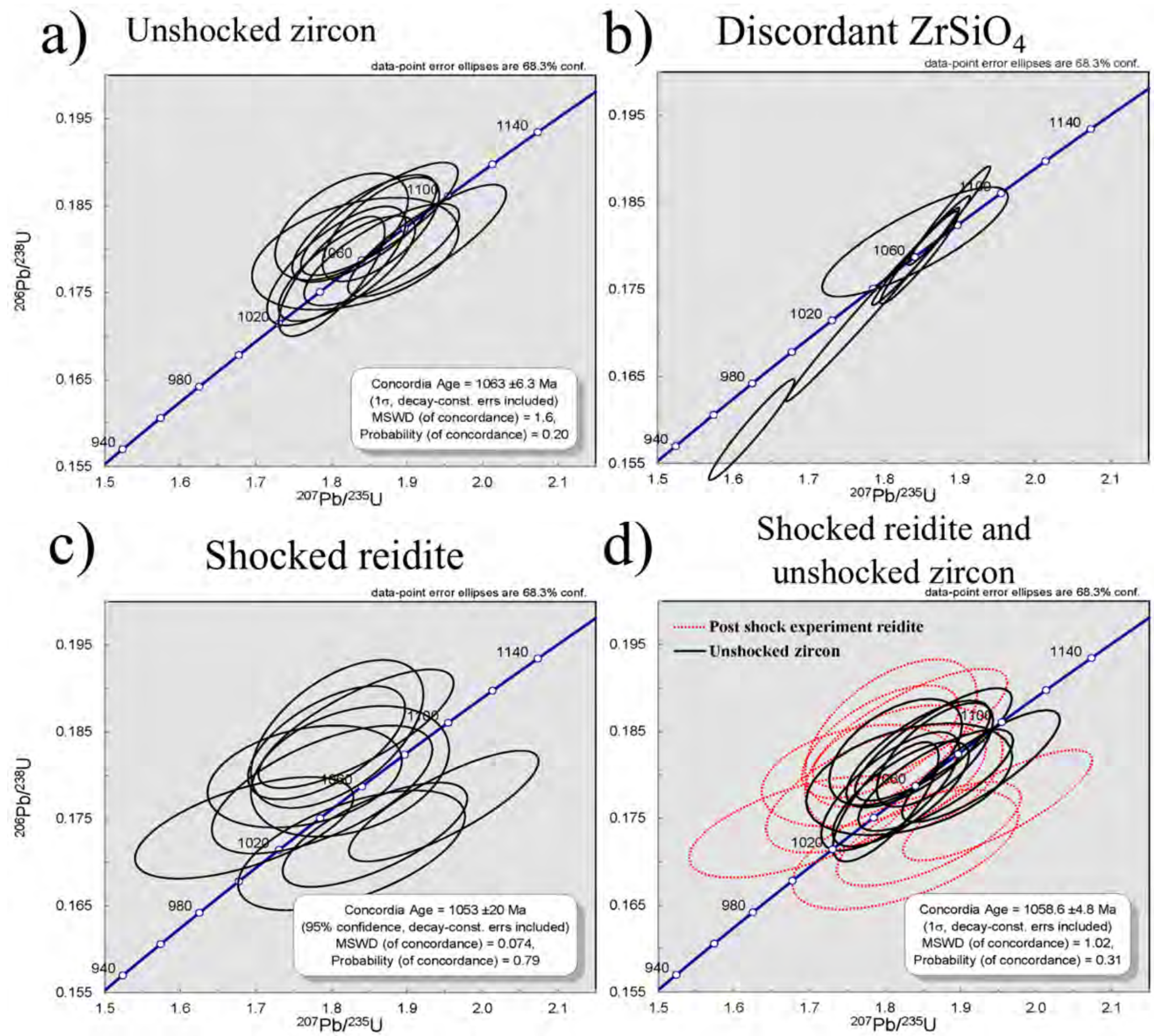

Figure 7. U-Pb concordia plots showing the $^{206}Pb/^{238}U$ and $^{207}Pb/^{235}U$ analyses from SIMS. The average age of the reidite is about 10 Ma younger than that of the unshocked intact zircon, but the two ages are overlapping within uncertainty. The slight difference in average age could be related to variations in the U content of the starting grain causing variations in Pb content between the unshocked zircon and the post-experiment reidite. The data from the reidite also tends to have larger uncertainty ellipses that the analyses from the unshocked intact zircon material. **(a)** SIMS analyses from unshocked zircon that still had intact crystal structure. This

was done by targeting these analyses on the crystalline zircon regions identified by the Raman mapping analysis shown in **Figure 3b**. **(b)** SIMS analyses on the unshocked fully metamict $ZrSiO_4$ material. These spot analyses were targeted using the spectral Raman map in **Figure 3** like before. **(c)** SIMS analyses of the post shock experiment reidite grain in **Figure 1** and named as grain A. **(d)** The SIMS analyses of the reidite (red dotted ellipses) and unshocked intact zircon (black solid ellipses) shown together.

Figure 8:

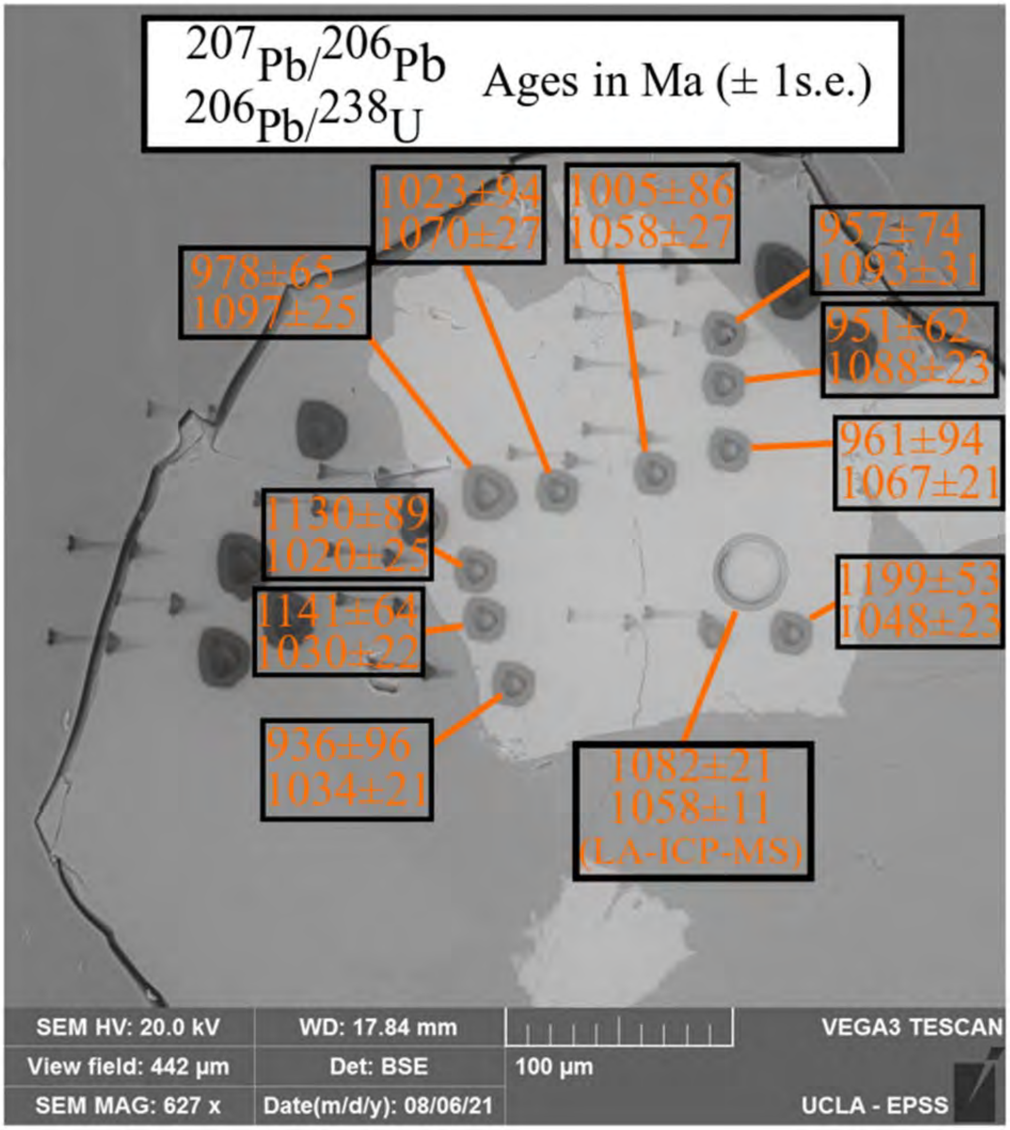

Figure 8. BSE image of post shock experiment reidite (grain A) and sanidine region. Spots are labeled with their $^{207}Pb/^{206}Pb$ and $^{206}Pb/^{238}U$ ages as measured by SIMS. One spot was analyzed by LA-ICP-MS rather than SIMS.

Figure 9a:

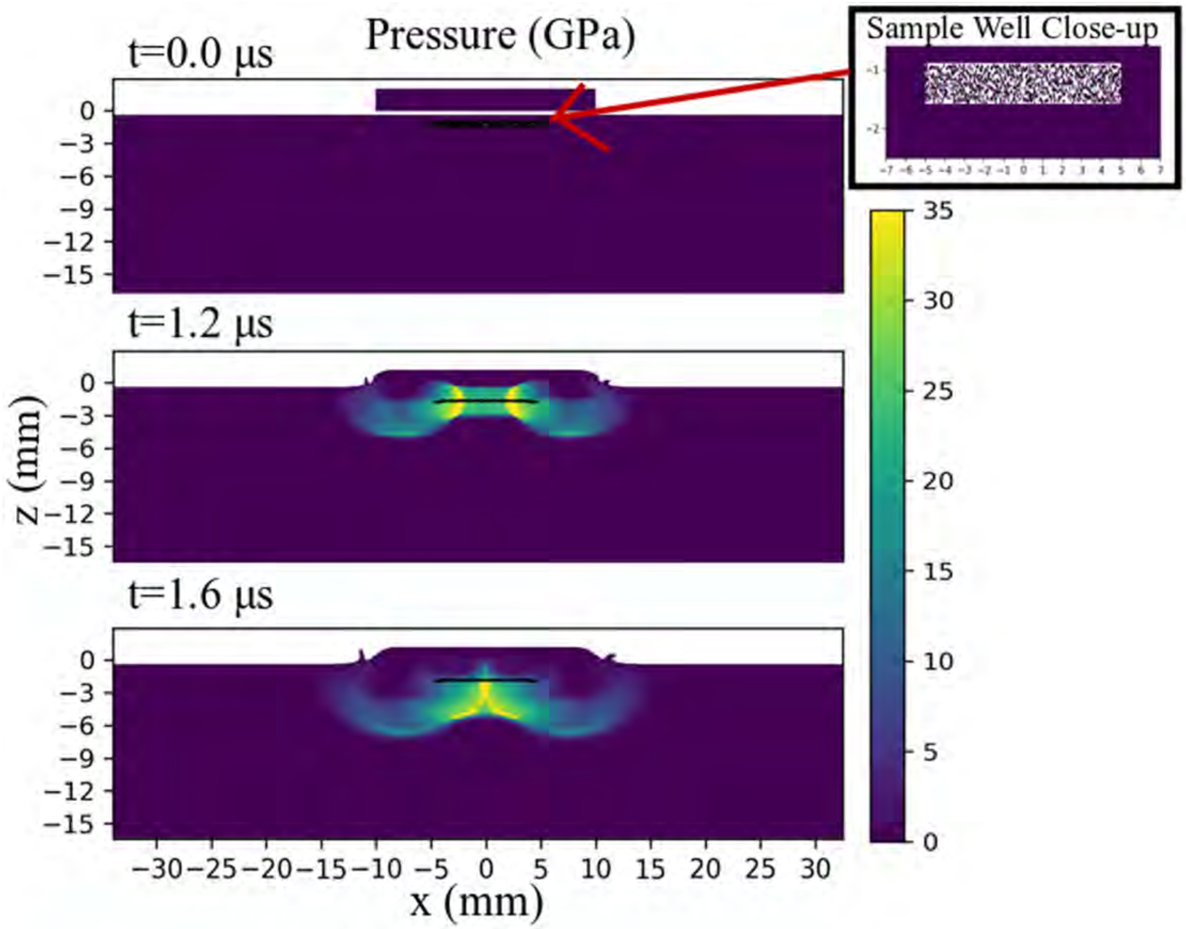
Pressure (GPa)
t=0.0 µs
t=1.2 µs
t=1.6 µs
Sample Well Close-up
z (mm)
x (mm)
0
−3
−6
−9
−12
−15
−30 −25 −20 −15 −10 −5 0 5 10 15 20 25 30
35
30
25
20
15
10
5
0

Figure 9b:

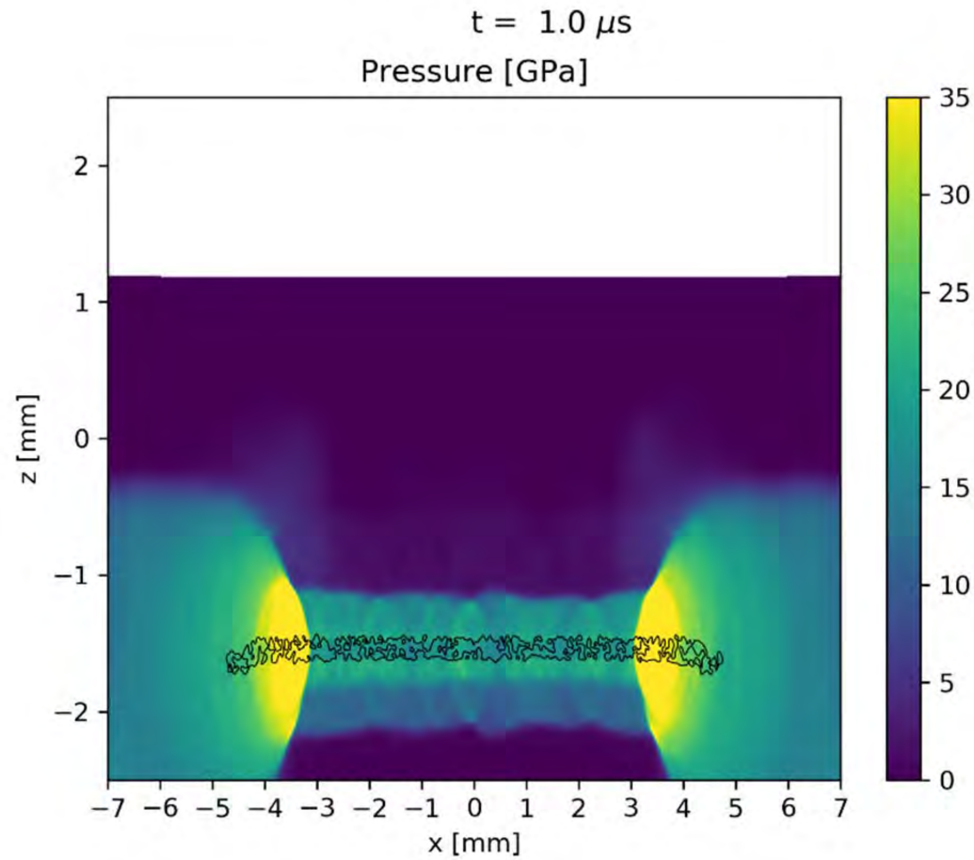
t = 1.0 μs
Pressure [GPa]
z [mm]
x [mm]
2
1
0
−1
−2
−7 −6 −5 −4 −3 −2 −1 0 1 2 3 4 5 6 7
35
30
25
20
15
10
5
0

Figure 9c:

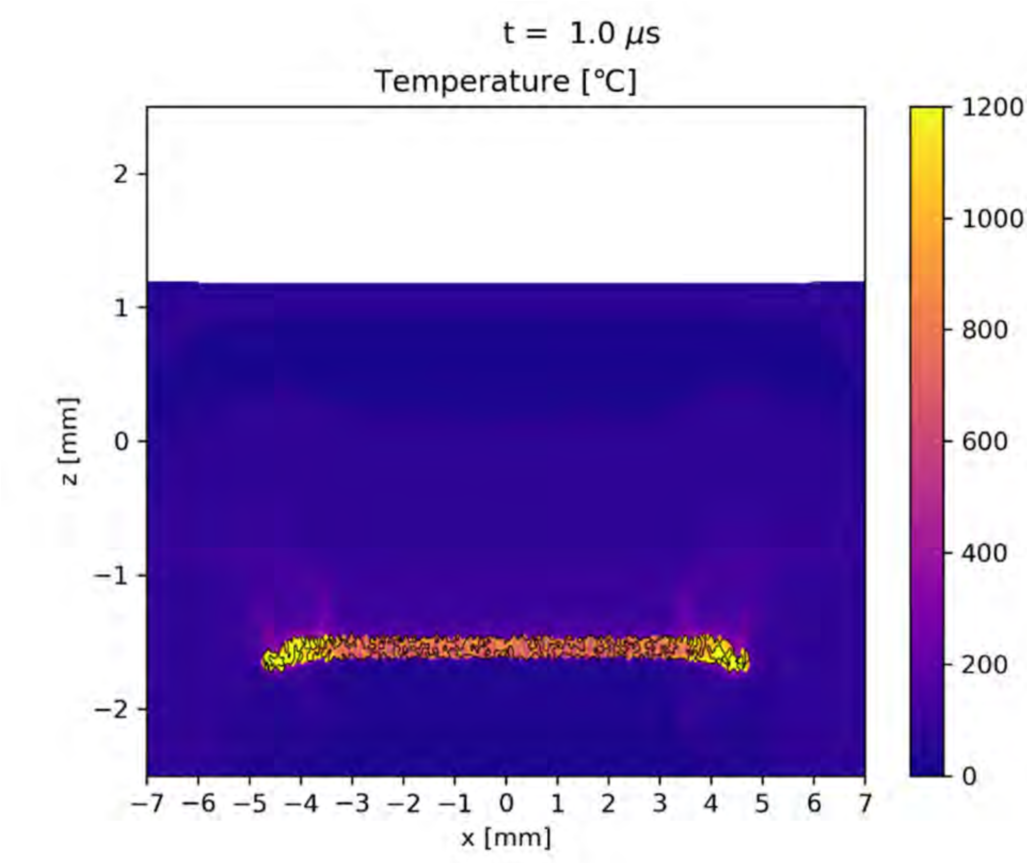

Figure 9 (a) The iSALE2D setup and simulation of the experiment with the sample material in the simulation just below the target, at the x axis center. The sample well is shown in the inset, populated with material at the start of the simulation. **(b)** A close-up view on the simulated sample well showing pressure at t=1.0 µs. **(c)** The same view but for temperature at t=1.0 µs.

Figure 10:

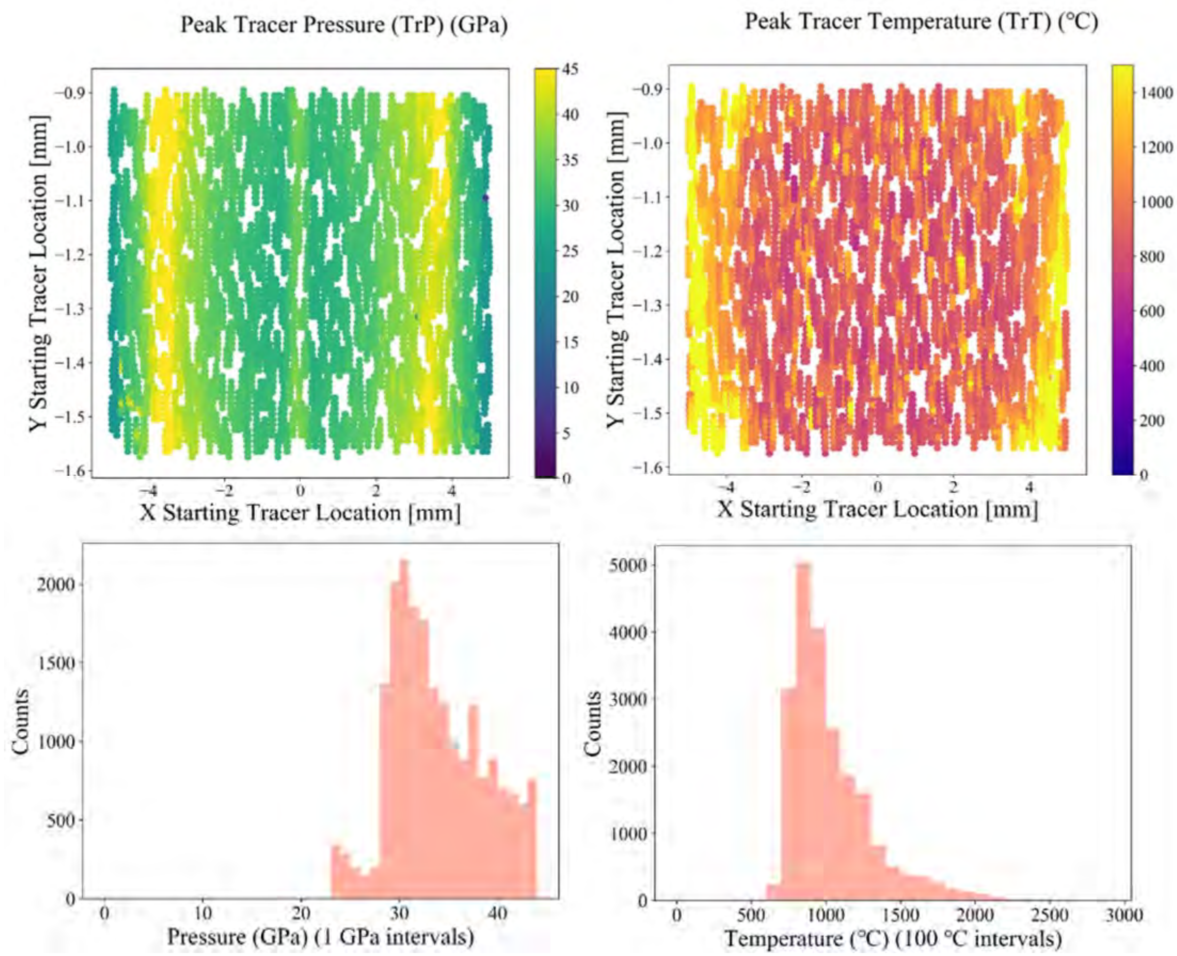

Figure 10. Plotted tracers representing peak *P* or *T* experienced at any point in the simulation. Histograms values are grouped into 1 GPa intervals for pressure and 100 °C intervals for temperature.